

Intimate Coupled Photocatalysis and Biodegradation

on a Novel TiO₂-Coated Biofilm Carrier

by

Guozheng Li

A Thesis Presented in Partial Fulfillment
of the Requirements for the Degree
Master of Science

Approved June, 2011 by the
Graduate Supervisory Committee:

Bruce Rittmann, Chair
Rolf Halden
Rosa Krajmalnik-Brown

ARIZONA STATE UNIVERSITY

August 2011

ABSTRACT

Intimate coupling of TiO₂ photocatalysis and biodegradation (ICPB) offers potential for degrading biorecalcitrant and toxic organic compounds much better than possible with conventional wastewater treatments. This study reports on using a novel sponge-type, TiO₂-coated biofilm carrier that shows significant adherence of TiO₂ to its exterior and the ability to accumulate biomass in its interior (protected from UV light and free radicals).

First, this carrier was tested for ICPB in a continuous-flow photocatalytic circulating-bed biofilm reactor (PCBBR) to mineralize biorecalcitrant organic: 2,4,5-trichlorophenol (TCP). Four mechanisms possibly acting of ICPB were tested separately: TCP adsorption, UV photolysis/photocatalysis, and biodegradation. The carrier exhibited strong TCP adsorption, while photolysis was negligible. Photocatalysis produced TCP-degradation products that could be mineralized and the strong adsorption of TCP to the carrier enhanced biodegradation by relieving toxicity. Validating the ICPB concept, biofilm was protected inside the carriers from UV light and free radicals. ICPB significantly lowered the diversity of the bacterial community, but five genera known to biodegrade chlorinated phenols were markedly enriched.

Secondly, decolorization and mineralization of reactive dyes by ICPB were investigated on a refined TiO₂-coated biofilm carrier in a PCBBR. Two typical reactive dyes: Reactive Black 5 (RB5) and Reactive Yellow 86 (RY86),

showed similar first-order kinetics when being photocatalytically decolorized at low pH (~4-5), which was inhibited at neutral pH in the presence of phosphate or carbonate buffer, presumably due to electrostatic repulsion from negatively charged surface sites on TiO₂, radical scavenging by phosphate or carbonate, or both. In the PCBBR, photocatalysis alone with TiO₂-coated carriers could remove RB5 and COD by 97% and 47%, respectively. Addition of biofilm inside macroporous carriers maintained a similar RB5 removal efficiency, but COD removal increased to 65%, which is evidence of ICPB despite the low pH. A proposed ICPB pathway for RB5 suggests that a major intermediate, a naphthol derivative, was responsible for most of the residual COD.

Finally, three low-temperature sintering methods, called O, D and DN, were compared based on photocatalytic efficiency and TiO₂ adherence. The DN method had the best TiO₂-coating properties and was a successful carrier for ICPB of RB5 in a PCBBR.

ACKNOWLEDGMENTS

I sincerely thank Dr. Bruce E. Rittmann for his patient guidance. It has been the most productive period in my life to work with him on such an interesting, exciting research topic in last two years. I also would like to thank two members in my graduation committee, Dr. Rolf Halden and Dr. Rosa Krajmalnik-Brown, for their time and suggestion.

I appreciated all the help from members of Swette Center for Environmental Biotechnology in Biodesign Institute, especially for Dr. Park who taught me hand-by-hand at the beginning of my research. I thank Chen Zhou, Yongneng Tang, Dae wook Kang, Hyun woo Kim, Michal Ziv-El, Prathap Parameswaran, Bradley Lusk, and Cesar Torres for their help on my research. It is more than pleasure to work with such a group of creative, kind, young scientists. I also appreciate the support and regulation from Diane Hagner and Dana Aguilar, who made my experiments go smooth and under control.

The study was supported by the US national Science Foundation (Grant No. 0651794). The sponge-type carrier used in this study was kindly provided by Samsung Engineering Co. Ltd, Korea. I was funded by Biological Design Graduate Program for my first-year study.

Last but not least, I would like to thank my family; I can't finish my study and this thesis with their support.

TABLE OF CONTENTS

	Page
LIST OF TABLES.....	vi
LIST OF FIGURES	vii
CHAPTER	
1 INTRODUCTION.....	1
2 2, 4, 5-TRICHLOROPHENOL DEGRADATION ON A NOVEL TIO ₂ COATED BIOFILM CARRIER: ROLES OF ADSORPTION, PHOTOCATALYSIS, AND BIODEGRADATION	5
Introduction.....	5
Material and Methods	8
Results and Discussion	18
Conclusion	32
3 DEGRADATION OF REACTIVE DYES IN A PHOTOCATALYTIC CIRCULATING-BED BIOFILM REACTOR.....	33
Introduction.....	33
Material and Methods	37
Results and Discussion	41
Conclusion	55
4 DEVELOPMENT OF AN EFFICIENT TIO ₂ -COAT BIOFILM CARRIER FOR INTIMATE COUPLING OF PHOTOCATALYSIS AND BIODEGRADATION	56

Introduction.....	56
Material and Methods.....	58
Results and Discussion.....	60
Conclusion.....	70
5 OVERALL CONCLUSIONS AND RECOMMENDATIONS.....	71
REFERENCES.....	73

LIST OF TABLES

Table		Page
1.	Experimental protocols for 2,4,5-TCP removal experiments	12
2.	Information on the reactive dyes	37
3.	Comparison of effluent and influent concentrations during RB5 degradation in the PCBRR	51
4.	Equivalent balances for proposed ICPB pathway and comparison to experimental values	51
5.	Comparison of the coating procedures	59
6.	First-order kinetic constants for RB5 photocatalytic degradation using carriers with the three sintering-based coating procedures	68

LIST OF FIGURES

Figure		Page
1.	The PCBBR	10
2.	SEM images of the exterior of the uncoated carrier and the TiO ₂ -coated carrier	18
3.	SEM images of exterior and interior the sponge carriers after cultivation.....	19
4.	SEM image of the carrier outer surface after biofilm cultivation and quantitative analysis of elemental distribution of selected region on the carrier by EDS.....	20
5.	Concentrations of 2,4,5-TCP in the PCBBR with different mechanisms acting: TCP adsorption, UV photolysis, UV photocatalysis, and biodegradation.....	21
6.	UPLC chromatograms of samples taken from the PCBBR at 1 hour showing intermediates from 2,4,5-TCP	22
7.	Equilibrium isotherm modeling of adsorption of TCP on the sponge carriers using the Freundlich isotherm	24
8.	PCBBR operation results	25
9.	SEM images of exterior and interior of the sponge carriers after 48 h and 240 h operation in the PCBBR	28
10.	Merged CLSM images and light micrographs of the same region after live/dead staining and CTC staining	29

Figure	Page
11. Pyrosequencing results from the activated sludge inoculum, cultivated biofilm, and after-operation sample	30
12. Adsorption and photocatalytic degradation of different dyes.....	42
13. RY86 adsorption and photocatalytic degradation with or without phosphate buffer	44
14. RB5 adsorption and photocatalytic degradation with phosphate, carbonate, and no buffer	45
15. RB5 degradation experiments in the PCBBR	48
16. SEM images of carriers and harbored bacteria at the end of the RB5 experiment in the PCBBR	49
17. Proposed decolorization and mineralization pathway of RB5 by ICPB in the PCBBR.....	50
18. Pictures of sponge-type carriers before and after TiO ₂ coating.....	60
19. SEM images of the carriers under 200X magnification and EDS elemental mapping of uncoated carrier and TiO ₂ -coated carrier by the O method.....	61
20. Elemental analysis by EDS of selected regions on uncoated carrier and TiO ₂ -coated carrier by the O method	61
21. SEM images of middle section of TiO ₂ -coated biofilm carrier	62
22. SEM images of interior and exterior of TiO ₂ -coated biofilm carrier (O method) after degrading 2,4,5-TCP after 34 days in the PCBBR	63

Figure	Page
23. SEM image and elemental mapping by EDS of biofilm carrier coated with TiO ₂ (O method) after TCP degradation experiment in the PCBBR.....	64
24. SEM images of uncoated carrier and TiO ₂ -coated carriers with O, D, and DN methods at 36-37X magnification	65
25. SEM image and titanium mapping by EDS of TiO ₂ -coated carriers with D method and DN method	66
26. SEM images of uncoated carrier and TiO ₂ -coated carriers with O, D, and DN methods at 200X magnification	66
27. RB5 adsorption and photocatalytic degradation using TiO ₂ -coated carriers prepared with the three different coating procedures	67
28. SEM images of biofilm carriers coated with TiO ₂ by the DN method after ~30-day PCBBR operation for degrading RB5.....	69

Chapter 1

INTRODUCTION

Synthetic organic compounds are extensively produced as herbicides, pesticides, surfactants, dyes, pharmaceuticals, and other industrial chemicals and by-products that are present in municipal and industrial wastewater (Nitschke et al., 1998; Rodgers et al., 2001; Chen et al., 2007; Sirtori et al., 2009). Many of these compounds are recalcitrant constituents that challenge conventional biological treatment systems and also pose severe health risks to humans and the environment (Staples et al., 1998; Valderrama et al., 2002; Aparicio et al., 2007). Advanced oxidation processes (AOPs) have been intensively investigated as robust means to remove biorecalcitrant organic compounds in water, as they have the potential to transform multiple refractory organics and reduce toxicity without the generation of sludge and by-products (Davis et al., 1994; Hofstadler et al., 1994; Nishio et al., 2006). The main technical barriers impeding the widespread use of AOPs include high energy/oxidant input, recovery of the catalyst particles, and incomplete mineralization (Horikoshi et al., 2003; Chong et al., 2010).

Biodegradation is the most extensively used method to treat wastewater and is less expensive than AOPs (Marsolek et al., 2008; Wang et al., 2009). Furthermore, biodegradation is able to completely mineralize the organics if they are not too recalcitrant or toxic. Recalcitrance and toxicity often are associated with complex aromatic structures and lack of specific enzymes in the microbial community (Faber et al., 1979; Cerniglia et al., 1992).

A promising approach for treating recalcitrant and toxic organics is to combine an AOP with biodegradation. The AOP can break the difficult structures by free radical attack, which can generate products that are readily biodegradable (Chong et al., 2010). Despite its obvious promise, the sequential arrangement of an AOP followed by biodegradation often does not work well, because the products generated by AOPs are diverse, with some oxidized more than necessary to be biodegraded or more toxic to the biomass (Marsolek et al., 2008).

An alternative approach is intimate coupling of photocatalysis and biodegradation (ICPB), which garners the benefits from AOPs and biodegradation while overcoming the above-mentioned barriers. In ICPB, photocatalysis and biodegradation occur simultaneously in the same reactor. Then, biodegradable products produced by photocatalysis are immediately biodegraded, which prevents them from being oxidized too much, wasting advanced oxidant, and possibly producing toxic products. The key to ICPB is protecting the microorganisms from UV light and free radicals by sheltering them as biofilm inside macroporous carriers that also have strong adherence of photocatalyst TiO_2 to the exterior surfaces.

Marsolek et al. (2008) demonstrated ICPB using a TiO_2 -coated cellulosic carrier to remove 2,4,5-trichlorophenol (TCP) in a photocatalytic circulating-bed biofilm reactor (PCBBR). Photocatalysis broke down TCP into biodegradable products that were simultaneously biodegraded and mineralized. Although successful for demonstrating ICPB, the cellulosic carriers used by Marsolek et al.

(2008) did not hold sufficient TiO₂ and were charred with prolonged use. Thus, a carrier more compatible with ICPB is needed. Ideally, an ICPB carrier should have a specific gravity similar to water for good circulation in the PCBBR, appropriately sized macropores for accumulating biomass and shielding them from UV/radical attack, significant and strong adherence of TiO₂ for photocatalytic reactions, and durability against abrasion for extended use.

Therefore, four primary objectives of this research on ICPB with the PCBBR are:

1. Investigate a new carrier for use in the PCBBR. This requires securing a novel carrier that meets goals of porosity, density, TiO₂ attachment capacity, and durability.
2. Test and compare the performance of the new carriers with the original model compound, 2,4,5 trichlorophenol (TCP), in the PCBBR.
3. Expand the capability of the PCBBR to target contaminants beyond TCP.
4. Utilize molecular microbial ecology to investigate how ICPB relates to the microbial community composition.

The remainder of this thesis is organized into four chapters. Chapters 2, 3, and 4 report on specific research projects to develop and test the novel carrier. Each of these chapters is adapted from manuscripts submitted for publication in

leading journals in environmental engineering and science. Chapter 2 shows that biorecalcitrant 2,4,5-trichlorophenol is effectively controlled by using ICPB occurring on the novel carrier. The chapter also demonstrates the profound influence of ICPB on the microbial community surviving in the interior of carriers. Chapter 3 documents ICPB for degrading and mineralizing a more challenging and complex organic compound—reactive black 5 (RB5) -- using an improved macroporous carrier at a low pH. Comprehensive experimental results make it possible to propose an RB5 degradation pathway that identifies and links the reactions brought about by photocatalysis and biodegradation. Chapter 4 compares three photocatalyst (TiO_2) coating methods developed to enhance ICPB. The results show that improving the homogeneity of the coated TiO_2 brings about more efficient photocatalysis and ICPB of RB5. Finally, Chapter 5 provides overall conclusions from the work and makes recommendations for promising next steps.

Chapter 2

2, 4, 5-TRICHLOROPHENOL DEGRADATION ON A NOVEL TiO₂-COATED BIOFILM CARRIER: ROLES OF ADSORPTION, PHOTOCATALYSIS, AND BIODEGRADATION¹

The worldwide expansion of the chemical industry has yielded products that benefit human society in many aspects, but wastes from generating and using the products cause a wide range of environmental problems, including bioaccumulation in and toxicity to humans and other organisms (Rodriguez et al., 2005; Feng et al., 2009). 2,4,5-trichlorophenol (TCP) is an important representative of chlorinated organic compounds that bioaccumulate, are toxic, and are extensively used as solvents, herbicide, pesticides, plastics, or their precursors (Schwien et al., 1988; Häggblom, 1992). Besides presenting human health risks by oral exposure, 2,4,5-TCP tends to bioaccumulate in the environment due to its biorecalcitrance in nature and in wastewater treatment plants (Agboola et al, 2005; ATSDR, 2004).

Even when some chlorinated compounds are biodegradable, their kinetics often are slow, and biodegradation occurs only at low concentration due to inhibition (Fava et. al, 1995; Dahlen and Rittmann, 2002a and 2002b; Marsolek et. al, 2007). In contrast, chemical oxidation is a robust method to break down large organic molecules, including aromatic compounds (Scott and Ollis, 1995).

¹ This chapter is adapted from a submitted paper: 2, 4, 5-Trichlorophenol Degradation Using a Novel TiO₂-Coated Biofilm Carrier: Roles of Adsorption, Photocatalysis, and Biodegradation. Li G, Park S and Rittmann BE. 2011. *Environ. Sci. Technol.*

However, full mineralization by chemical oxidation is economically prohibitive, and the products from partial chemical oxidation retain toxicity and oxygen demand (Belhacova et al., 1999). An emerging approach combines chemical oxidation and biodegradation to overcome the limitations of both methods (Scott and Ollis, 1995 and 1996). In such combined treatment, chemical oxidation partially transforms biorecalcitrant organic compounds into intermediates that can be fully mineralized by biodegradation (Bandara et al., 1997; Marsolek et al., 2008).

Most prior attempts at combined treatments applied an advanced oxidation process (AOP) and biological treatment separately; this is called *sequential coupling* (Marco et. al, 1997; Hong and Zeng, 2002). AOPs rely on free-radical reactions, which are indiscriminate in most cases, producing a range of products that can be excessively oxidized or not readily biodegradable. Excessive oxidation wastes oxidant and increases treatment costs, and poor biodegradability defeats the goal of downstream biodegradation.

The problems of sequential treatment can be overcome if the AOP and biodegradation occur together; this is called *intimate coupling*. Marsolek et al. (2008) successfully demonstrated the concept of intimate coupling of photocatalysis and biodegradation (ICPB) for 2,4,5-TCP in a novel photocatalytic circulating-bed biofilm reactor (PCBBR) that exploited macro-porous cellulose carriers. Titanium dioxide (TiO₂) particles were either fixed onto the outer surface of biofilm carriers or circulated in slurry form. When illuminated with

UV light, the TiO₂ photocatalyzed TCP into intermediates that could be biodegraded by bacteria in a biofilm inside the macroporous carriers, where the bacteria were protected from UV light and free radicals generated as part of photocatalytic advanced oxidation.

The carriers used by Marsolek et al. (2008) were made of cellulose. While they had good wet density for circulation and macropores ideal for biofilm accumulation, they were charred by UV irradiation and hydroxyl radical attack. This charring eventually led to a deterioration of the carriers' physical structure. Therefore, the biofilm-carrier needs to be made of a material better suited to intimate coupling with an AOP. An ideal carrier for ICPB should have porosity suitable for accumulating biofilm inside, a density allowing good circulation in the reactor, the ability to hold a substantial amount of TiO₂, and durability for long-term use in the PCBBR.

In this study, we tested a new sponge-type carrier for its physical properties, TiO₂-coating capacity, and ability to harbor biofilm. We evaluated 2,4,5-TCP degradation by ICPB in the PCBBR using this carrier by tracking the TCP concentration, major intermediates, dissolved organic carbon (DOC), and the microbial community. We determined the roles of four mechanisms that affect intimate coupling: TCP adsorption to the carrier, UV photolysis, UV photocatalysis, and biodegradation for different operating conditions in the PCBBR. We also assessed the impact of ICPB on the microbial community.

Materials and Methods

Carrier

We used a commercially available macroporous sponge cube, BioCAP[®] (Samsung Engineering Co., Ltd. Seoul, Korea), as the carrier in our experiments. The sponge-type carrier was made of polyurethane and had an average side length of 3.5 mm. The manufacturer reports that the carrier has a high specific surface area of 4.8 m²/g by BET measurement (Brunauer et. al., 1938), high porosity (88%), and a wet density close to that of water (1.01-1.02 g/cm³).

Titanium Dioxide Coating Procedure

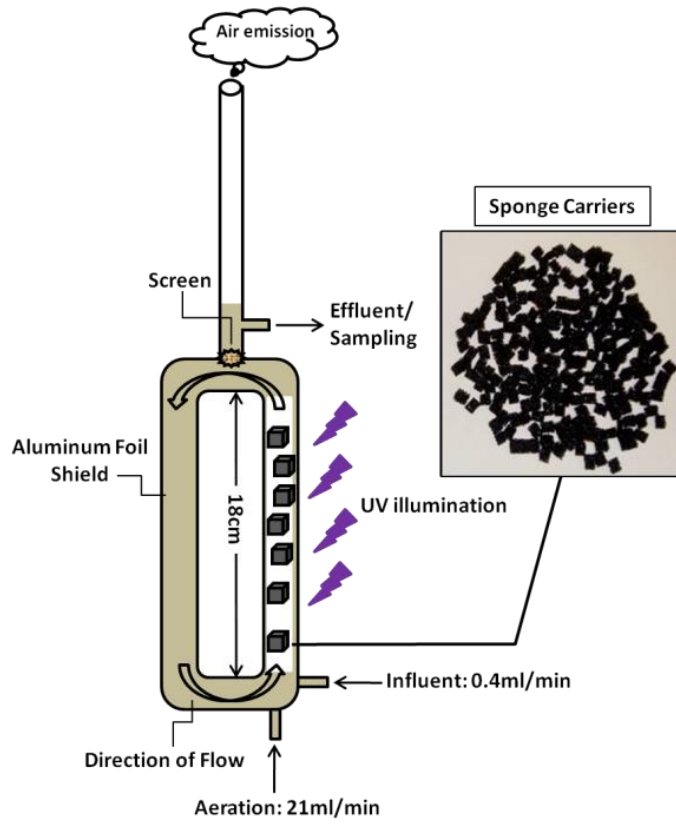
We coated the carrier with TiO₂ using a sintering method modified to prevent the melting or charring that would occur with normal high-temperature sintering (>550 °C) (Cannon et al. 2005). Titanium isopropoxide (Alfa Aesar, Ward Hill, MA, USA) was added to 150 mL of 0.075 M nitric acid (Sigma-Aldrich, St. Louis, MO, USA) to give 6.7 g of TiO₂ in solution. After nitric-acid addition was completed, we decreased the solution volume to 50 mL by heated it at 80 °C. Then, we cooled the solution to room temperature and added 5% 1,3,5-benzenetricarboxylic acid (trimesic acid, 98%, Alfa Aesar, Ward Hill, MA, USA). Covering the beaker with aluminum foil, we raised the solution's temperature in an oil bath to 130 °C for 18 hours and then cooled the resulting suspensions to room temperature. Finally, we added 10 gram uncoated sponge carrier to the coating solution and incubated the mixture in an 80 °C oven for 5 hours (with mixing every 30 minutes) until all liquid was evaporated so that the TiO₂ was coated on the carrier.

We then rinsed the coated carriers (after the carriers cooled down to room temperature) to remove any poorly fixed TiO₂. We conducted 3 rinses with 500 mL of autoclaved deionized water for 3 minutes each, and then we dried the carriers in a 105 °C oven before weighing to assess the amount of attached TiO₂. The loss of TiO₂ was less than 5% loss during the rinsing process, which indicates that the TiO₂ was strongly attached.

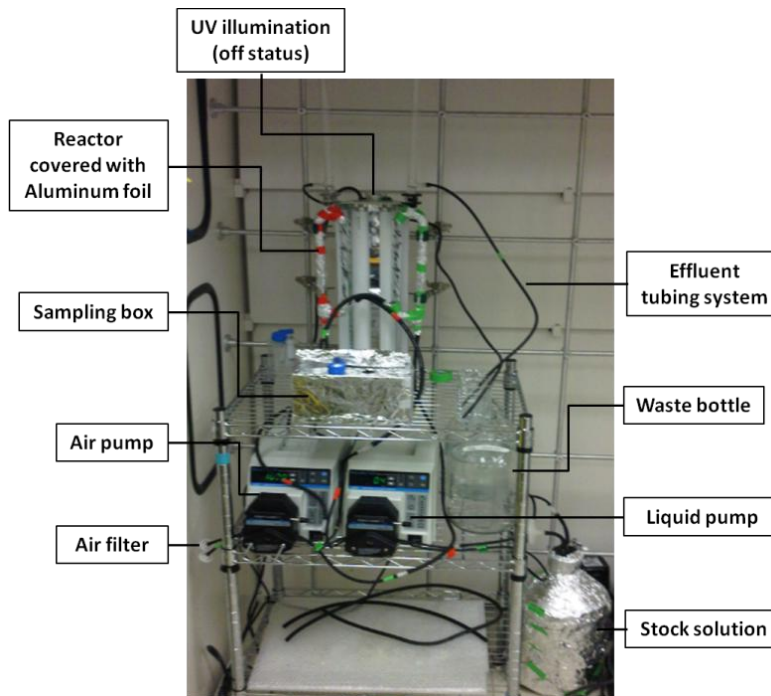
Reactor Set-Up

The bench-scale PCBBR, shown in Figure 1, was made of quartz glass (2-cm inner diameter) and had a liquid volume of 150 mL, with roughly equal volumes in the riser and down-comer sides. The PCBBR was covered with aluminum foil, except for an 18-cm length on the riser side, where UV light could enter.

Circulation of water and carriers was achieved by bubbling filtered air at the bottom. Bubbles rising up the riser side created an air-lift pump and also provided oxygen for photo(cata)lytic oxidation and biodegradation. The air was supplied by the Masterflex L/S pump and L/S 14 tubing system (Cole-Parmer, Vernon Hills, Illinois, USA) at an aeration rate of 21 mL/min and sterilized through 0.2 µm PVDF filter (Whatman, Piscataway, NJ, USA) prior to entering the reactor. The long neck at the top of the reactor was used to condense water vapor and minimize water loss by evaporation.



(a)



(b)

Figure 1. The PCBBR: (a) schematic diagram and (b) photograph.

The influent was pumped into the reactor through a Masterflex L/S pump from a 10-L bottle filled with synthetic medium consisting of 50 μM 2,4,5-TCP (95%, Sigma-Aldrich, St. Louis, MO, USA) and mineral components: 1.8 mM $(\text{NH}_4)_2\text{SO}_4$, 45.0 μM CaSO_4 , 0.6 μM FeCl_3 , 4.2 μM $\text{MgSO}_4 \cdot 7\text{H}_2\text{O}$, 1.6 μM $\text{MnSO}_4 \cdot \text{H}_2\text{O}$, and 24.3 nM Na_2MoO_4 in MilliQ water (Marsolek et al., 2008). The influent was supplied with the rate of 0.4 mL/min, which provided a hydraulic retention time (HRT) as 6 h. The carrier loading was 0.5 gram as dry weight, and the carriers were pre-soaked with autoclaved deionized water to remove the air from the pores for good circulation in the reactor.

The PCBBR was illuminated with two UV lamps (100W Longwave, UVP Inc., Upland, CA, USA) giving an intensity was 3.0 mWatt/cm² as measured with a UV513AB digital UV meter (General Tools & Instruments Co., New York, NY, USA). With 18-cm exposed length, the total exposed volume for irradiation was approximately 57 cm³, which was 38% of total liquid volume of the reactor. The entire system was operated in a shielded hood for eye protection.

Inoculum and Cultivation

Biofilm was cultivated onto the carriers by immersing them in activated sludge collected from the Northwest Water Reclamation Plant (Mesa, Arizona, USA). The activated sludge had a volatile suspended solids concentration of 3,000 mg/L to begin, we fed it 5-fold concentrated Luria-Bertani (5 \times LB) medium (Sambrook and Russell, 2001) every two days, and it was mixed on rotary shaker at 150 rpm

and with a temperature of 30 °C. We collected 4 carriers before PCBBR operation for monitoring the microbial community components.

Short-Term PCBBR Operation and TCP Adsorption Test

The mechanisms acting during the intimate coupling in the PCBBR were evaluated in a set of four experiments: (1) uncoated carriers without UV illumination to evaluate TCP adsorption; (2) uncoated carriers with UV light to evaluate the combined effect of adsorption and photolysis; (3) TiO₂-coated carriers to evaluate the combined effect of adsorption, photolysis, and photocatalysis; and (4) carriers with TiO₂ coating with UV light and cultivated biofilm to analyze the intimate coupling of adsorption, photo(cata)lysis, and biodegradation. Table 1 lists the detailed conditions for the different experiments.

Table 1

Experimental protocols for the experiments for 2,4,5-TCP removal

Exp. #	Removal impact factors	TiO ₂ coating	UV	Biofilm
1	AD	–	–	–
2	AD+PL	–	+	–
3 (PC)	AD+PL+PC	+	+	–
4 (PBC)	AD+PL+PC+BD	+	+	+

AD, Adsorption; PL-photolysis; PC-photocatalysis; BD-biodegradation; PBC-photobiocatalysis. +, applied; –, not applied.

Separate batch TCP-adsorption experiments were conducted by using 250-mL beakers covered with aluminum foil to minimize evaporation and light effects.

Each beaker contained 0.5 g carriers in a 150-mL TCP solution with a series of concentrations (5, 10, 25, 50, and 100 mg/L as DOC). Each beaker was placed on a VWR 620 Standard Magnetic Stirrer (120V, 50/60Hz, 0.5A, 50W, Radnor, PA, USA) and mixed with a 2-cm stir bar at ~ 25°C, the same as the PCBBR operating temperature. Liquid samples were taken after 6 hour and 24 hour and filtered through 0.2- μ m syringe filters before DOC analysis.

Sampling and Analytical Methods

We collected effluent samples from the outlet of the PCBBR through Masterflex L/S 14 tubing. The tubing and sample container were shielded by aluminum foil to avoid exposure to UV irradiation. Influent samples also were obtained periodically by removing liquid sample from the influent reservoir with a pipette. We measured pH with an Accumet® AB15 Basic pH/mV Benchtop Meter (Cole-Parmar, Vernon Hills, Illinois, USA) and then filtered the samples through a 0.2- μ m PVDF membrane filter. The filtered samples were analyzed for concentrations of the 2,4,5-TCP and intermediates by Ultra-Performance Liquid Chromatography (UPLC) system (WATERS, Milford, MA, USA) with ACQUITY UPLC column of 2.1 \times 50 mm, 1.7 micron BEH C₁₈. The mobile phase was an acetonitrile-in-water gradient from 30 to 70% acetonitrile at a flow rate of 0.6 mL/min. Solvents for UPLC analysis were of LC/MS grade (Fisher Scientific, Fair lawn, NJ, USA). The detector was a photo diode array (PDA) with a detecting wavelength of 290 nm. The retention time of 2,4,5-TCP was 1.17 – 1.19 min. Samples (5 μ L for each injection) were withdrawn automatically

by the Sample Manager. DOC was analyzed by a Total Organic Carbon Analyzer (DOC-UCPH/CPN, Shimadzu, Kyoto, Japan). Cl^- was analyzed with an ion chromatograph (ICS-2000, Dionex, Sunnyvale, CA, USA) using a conductivity detector.

We periodically removed carriers from the reactor to monitor their physical properties, accumulation and activity of biomass, and microbial community. Carriers were collected by removing the neck of the reactor, removing the screen, and retrieving cubes with a sterilized tweezers. The collected carriers were immediately placed either in (1) 4.0% paraformaldehyde solution for further Scanning Electron Microscopy (SEM) analysis; (2) Live/Dead or CTC (5-cyano-2,3-ditolyl tetrazolium chloride) stain for confocal laser scanning microscopy (CLSM); or (3) 2.0-mL tubes (Eppendorf Canada, Mississauga, Ontario, Canada) at -80°C for bacterial community analysis.

Scanning Electron Microscopy

Microorganisms on the carriers were fixed in 4% solution of paraformaldehyde, processed through an ethanol dehydration series (i.e., 25%, 50%, 75%, 100% v/v ethanol, 0.25 h each treatment), and transferred into acetone three times, 0.25 h per time. The carriers were further dried in a Tousimis 815 AutoSamdri critical point dryer (Tousimis Inc., Rockville, MD, USA) to preserve the structure of the microbes. The treated samples were coated with gold and visualized at 20kV with an XL30 environmental field emission SEM (FEI, Hillsboro, Oregon, USA). Interiors were visualized by slicing the carriers with a sterile razor blade prior to

gold coating. We performed energy dispersive X-ray spectroscopy (EDS) for elemental mapping with a PGT energy dispersive X-ray analyzer on the S-3500N.

Confocal Laser Scanning Microscopy

We acquired confocal laser scanning microscopy (CLSM) images using a Zeiss LSM 510 camera (Carl Zeiss, Jena, Germany). Carriers removed from the reactor were immediately placed in a Live/Dead stain (Live/Dead BacLight Bacterial Viability Kit, Molecular Probes Inc., Eugene, OR, USA) or CTC stain (BacLight RedoxSensor CTC Vitality Kit, Molecular Probes Inc., Eugene, OR, USA). Some carriers were cut into half prior to staining if the interior was observed. After staining, carriers were placed on a glass slide, submerged with water, and visualized by using an air lens (10X/0.3NA).

Genome DNAs Extraction and PCR Diagnosis

We employed a PowerSoil™ DNA isolation kit (MO BIO laboratories, Inc., USA) to extract genomic DNA from biofilm on the carriers and in the original activated sludge. The amount of extracted sample was 4 cubes for the carriers and 0.5 g (dry weight) for the activated sludge. The concentrations and quality of extracted genome DNAs were measured by a NanoDrop 1000 spectrophotometer (Thermo Fisher Scientific Inc., Wilmington, DE, USA). 2- μ L DNA samples were used to make 1:10 and 1:100 dilutions for PCR diagnosis, which confirmed that extracted genomic DNA was amplifiable. We stored the remainder in 1.5-mL tubes (Eppendorf Canada, Mississauga, Ontario, Canada) at -80°C for pyrosequencing.

We PCR amplified the 16S rDNA for general bacteria using the universal bacterial primers 8F and 1525R (Lee et al., 2008). 20- μ L reactions were performed in a thermocycler (Matercycler, Eppendorf, Westbury, NY, USA) with 2- μ L template solution, 0.2 μ L each of forward and reverse primers (10 μ M), 2 μ L magnesium solution, 10 μ L Taq PCR Master Mix (QIAGEN), and 5.6 μ L PCR-grade water. The PCR thermal program was set at 92 $^{\circ}$ C for 2 min, followed by 30 cycles at 94 $^{\circ}$ C for 30 sec, 55 $^{\circ}$ C for 45 sec and 72 $^{\circ}$ C for 2 min, followed by a final extension at 72 $^{\circ}$ C for 10 min. The amplified DNA was then stored at 4 $^{\circ}$ C. Electrophoresis of all samples was conducted by applying 5 μ L of each PCR product on 1% agarose gel and employing a voltage difference of 100V for 30 minutes.

Pyrosequencing and Analysis of Community Structures

We sent extracted genomic DNA to the Research and Testing Laboratory (Lubbock, TX, USA), where bacterial-tag-encoded FLX amplicon pyrosequencing (bTEFAP) was performed by the Genome Sequencer FLX-Titanium System and its Titanium protocol (Roche, Indianapolis, IN). We selected bacterial primers 104F (5'-GGCGVACGGGTGAGTAA-3') and 530R (5'-CCGCNGCNGCTGGCAC-3') to amplify the combined V2 and V3 regions of 16S rDNA, and the amplicon was sequenced by the procedure described by Wolcott et al. (2009). Using the Mothur software (Schloss et al, 2009), we trimmed of barcodes and primers and then eliminated all failed and low quality pyrosequencing reads (Huse et al., 2007). We aligned all qualified sequences by

using the Silva alignment (Pruesse et al., 2007) and excluded sequences shorter than 200 bp and chimeric sequences detected by modified ChimeraSlayer (Hass et al., 2011). We clustered the sequencing readouts at 97% similarity with the farthest algorithm to obtain the number of unique phylotypes and calculated rarefaction curves with the help of the Mothur software. Finally, we classified sequences by the RDP Classifier software at the 50%-confidence threshold (Cole et al., 2009).

Results and Discussion

TiO₂-Coated Sponge Carrier and Its Biofilm Cultivation

One of the major objectives of this work was to find a carrier that has good circulation in the PCBBR and significant and strong adherence of TiO₂. The circulation characteristic is determined primarily by the mass density, and the wet density of 1.01 – 1.02 g/cm³ allowed excellent circulation for the uncoated and TiO₂-coated carriers. After attachment using the modified sintering method, the TiO₂ density on the carriers was approximately 0.5 g/g based on the dry-weight increase; this value is almost ten times greater than the 0.06 g/g that achieved by Marsolek et al. (2008) using a sol-gel technique. Figure 2, which shows the SEM images of the uncoated sponge carrier and TiO₂-coated carrier, confirms that small blocks of TiO₂ were scattered over the surface of the sponge carrier.

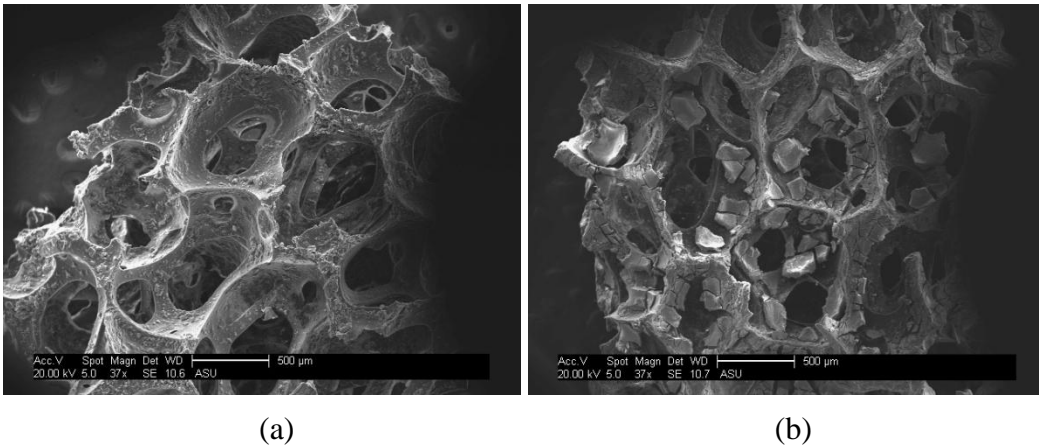


Figure 2. SEM images of the exterior of (a) uncoated carrier and (b) TiO₂-coated carrier. The blocks of coating particles are evident in (b).

Accumulation of sufficient active biomass inside the coated carriers is another crucial condition for ICPB. Figure 2 shows that macropores, essential for

bacteria to migrate inside the carrier, remained in the carriers after TiO₂ coating. The SEM images in Figure 3 prove that biomass accumulated well on the exterior and interior of coated carriers before exposure to UV light. The external surface showed higher biomass density, presumably due to the need for the bacteria to penetrate into the carriers. Another important requirement is that the bacteria did not dislodge the TiO₂ from the carrier surface. Figure 4 clearly shows that coated TiO₂ remained well attached to the carriers after the biomass-cultivation process. Thus, the TiO₂-coated carriers held considerable TiO₂ and biomass, meeting the basic requirements of ICPB.

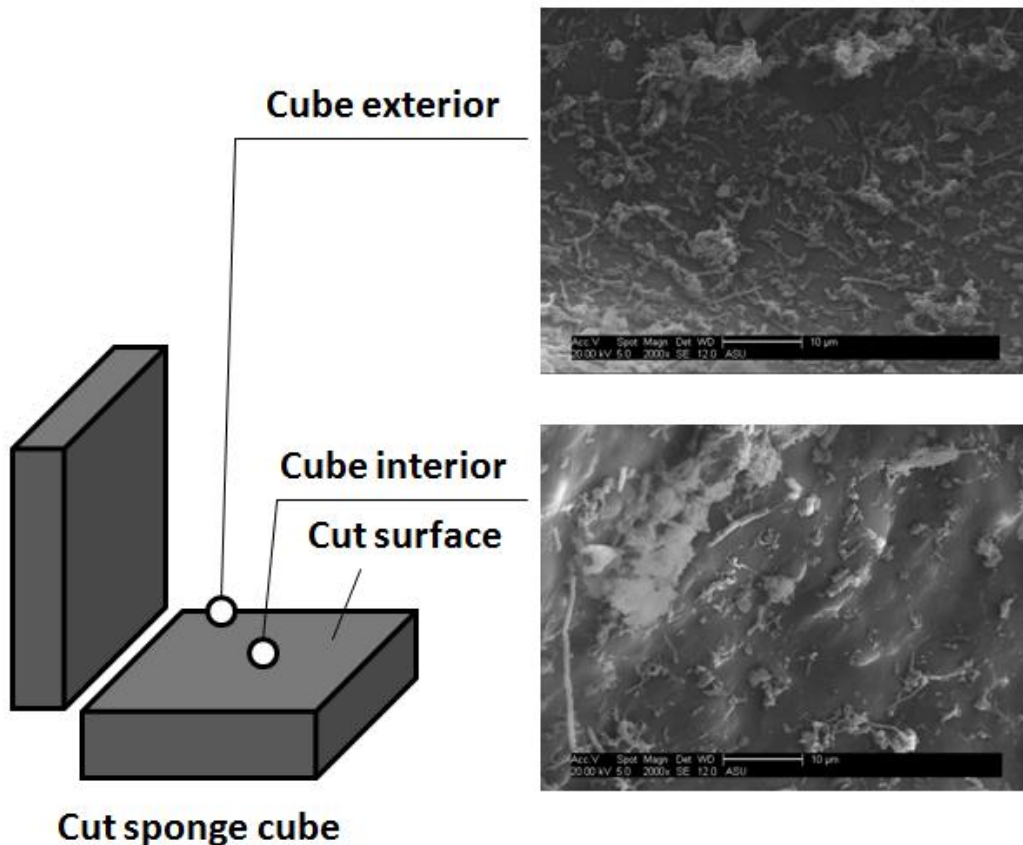


Figure 3. SEM images (2000X magnification) of exterior (top) and interior (bottom) the sponge carriers after cultivation.

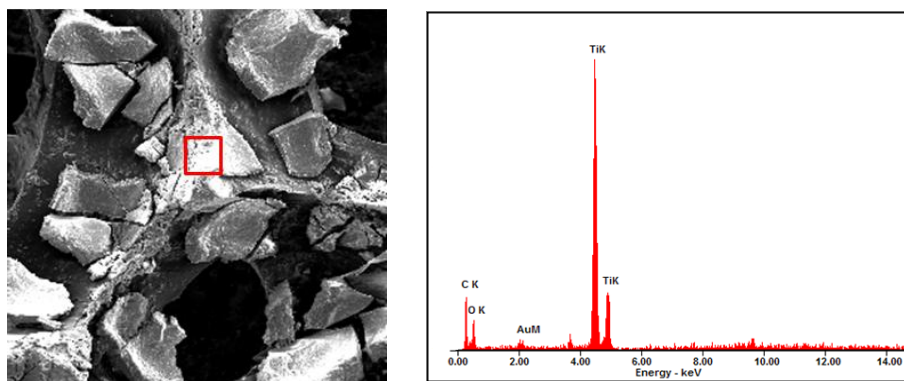


Figure 4. SEM image (200X magnification) of the carrier outer surface after biofilm cultivation (left) and quantitative analysis of elemental distribution of selected region (shown by the red square) on the carrier by EDS.

Mechanisms and Intermediates of ICPB

Four mechanisms --TCP adsorption, UV photolysis, UV photocatalysis, and biodegradation -- could contribute on the removal of 2,4,5-TCP from the bulk solution in an ICPB process. To understand the roles of each effect in the PCBRR, we separately conducted short-term experiments (24 hours) using the four different conditions summarized in Table 1. Figure 5 shows effluent concentrations of 2,4,5-TCP for the 24-hour batch experiments.

Although others have reported that photolysis breaks down TCP (Skurlatov et al., 1997; Zhang et al., 2010), we did not observe any evidence of this in experiment 2 (adsorption + photolysis). The rate of TCP loss was not faster than with adsorption alone, and UPLC chromatograms in Figure 6a showed no detectable intermediates during UV treatment. The lack of effect of photolysis probably occurred because fast adsorption transferred most of the TCP from the liquid phase to the interior of the carrier matrix, leaving little TCP for UV photolytic reaction.

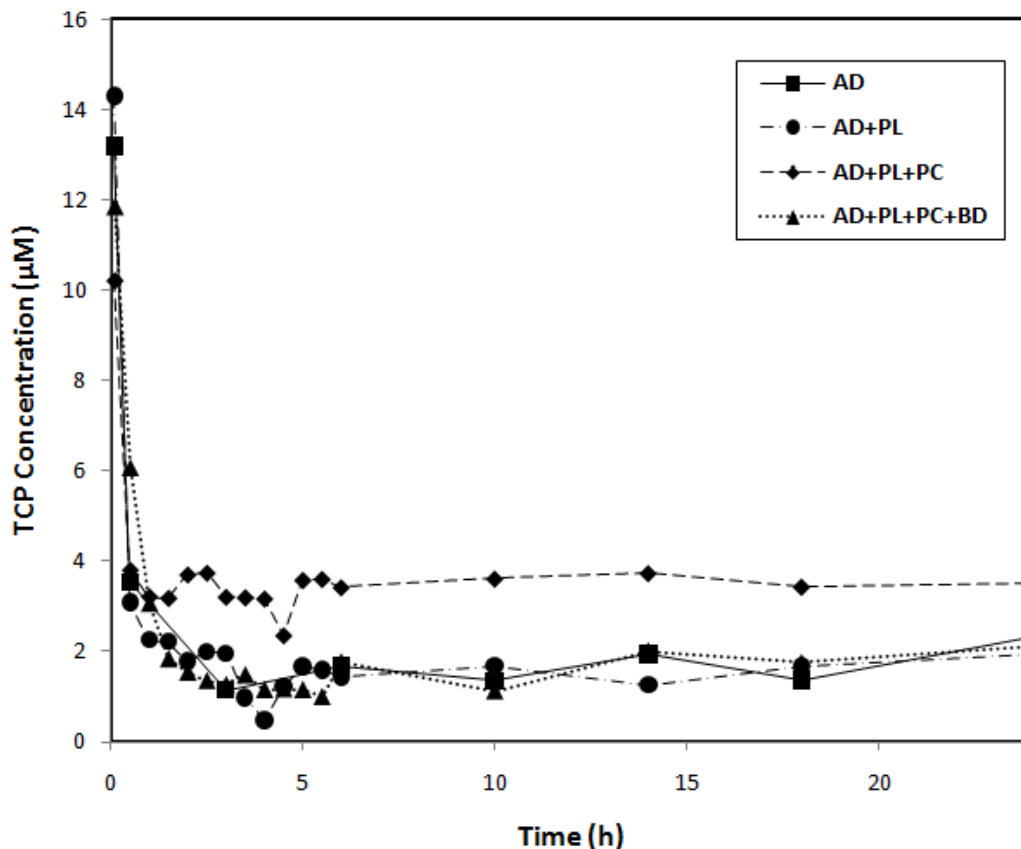


Figure 5. Concentrations of 2,4,5-TCP in the PCBRR with different mechanisms acting: TCP adsorption (AD), UV photolysis (PL), UV photocatalysis (PC), and biodegradation (BD). The starting concentration, 50 μM for each experiment, is not shown in order to improve visualization of the concentrations from 0.1h.

By the first sampling time of 0.1 h, the sponge carriers displayed significant adsorption of TCP from the starting TCP concentration of 50 μM . 92% removal was achieved in the first hour of experiment 1 (adsorption alone), and the aqueous-phase TCP decreased to approximately 2 μM when the system approached equilibrium at 24 hours.

Compared to uncoated carriers, TiO_2 -coated carriers showed slightly slower TCP adsorption in experiment 3, with 92% removal of TCP in 1 hour. This probably was caused by the TiO_2 coating, which blocked some adsorption

sites on the carriers. Although adsorption dominated removal, evidence of photocatalysis is present in the UPLC chromatogram of Figure 6b, which shows one major intermediate (at 0.18 min).

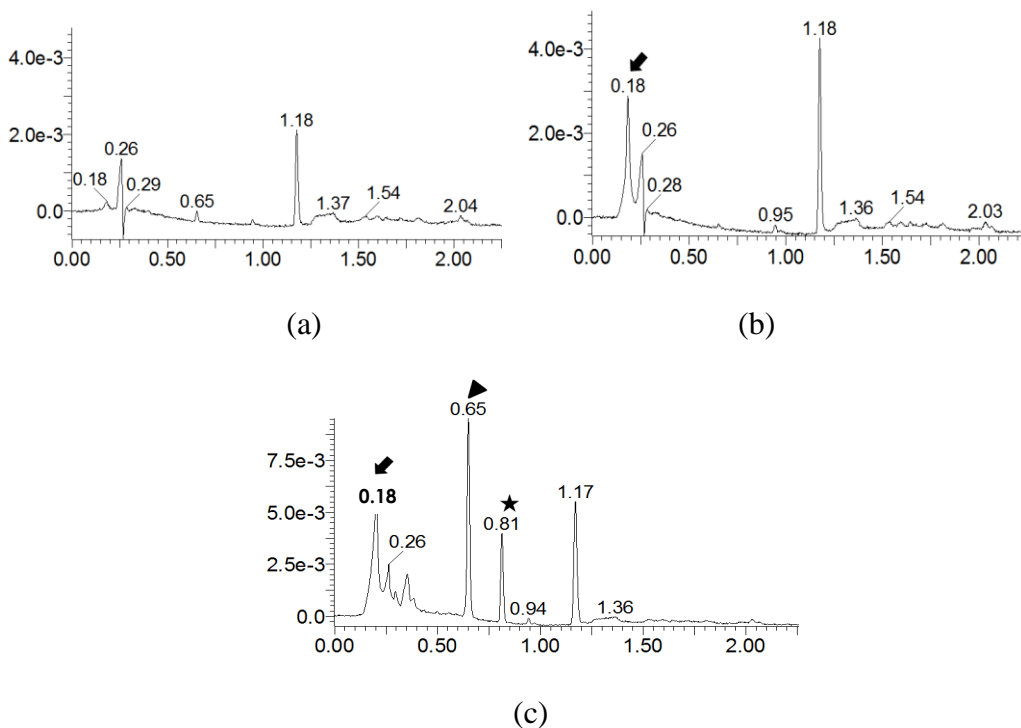


Figure 6. UPLC chromatograms of samples taken from the PCBRR at 1 hour show intermediates from 2,4,5-TCP. The retention time in minutes is shown above a peak. The peaks at 1.17-1.18 min represent the original TCP. The peak at 0.26 min is a background signal that appears on all chromatograms. Peaks occurring before 1.17 min are intermediates from TCP decomposition. (a) No large peaks appear with photolysis (exp. 2). (b) The large peak at 0.18 min is characteristic of photocatalysis (exp. 3). (c) Three intermediates associated with intimate coupling (exp. 4) are at 0.18, 0.65, and 0.81 min.

Adding biodegradation in experiment 4 further slowed TCP adsorption, with only 88% removal in 1 hour; thus, biomass on the surface and inside of carriers also appears to have blocked TCP adsorption sites. However, the TCP concentration in the liquid phase decreased later in the experiment, ending at 1.5

μM , which was slightly lower than with uncoated carriers. Probably biodegradation contributed directly to the loss of TCP and to recovering adsorption sites. This concept is supported by the detection of three intermediates in the liquid phase (Figure 6c). Since TCP is highly biorecalcitrant at $50 \mu\text{M}$ (Marsolek et al., 2007), TCP biodegradation may have been aided by strong adsorption, which lowered its concentration to a non-inhibitory level.

Adsorption isotherm of sponge carriers

Because of the important role of adsorption, we conducted TCP-adsorption experiments to generate an adsorption isotherm for the sponge carriers. An equilibration time of 6 hours was used, as the concentration did not change for longer times (data not shown). Figure 7 presents the adsorption density versus equilibrium concentration measured as DOC. Since the adsorption density showed no plateau, we did not attempt a Langmuir isotherm, but fit a Freundlich isotherm: $Q = 0.32C^{1.93}$, in which Q is the TCP adsorption density (mg DOC/g carrier), and C is the TCP equilibrium concentration (mg DOC/L). The exponent is nearly equal to 2, which corresponds to so-called unfavorable adsorption (Ribeiro et al., 2001; Grushka et al., 2007), because adsorption sites have a relatively high energetic barrier that results in slow lateral diffusion. In this case, adsorption becomes stronger for higher concentrations of 2,4,5-TCP, and this benefits biodegradation by reducing bulk-liquid TCP concentration when inhibition is most important.

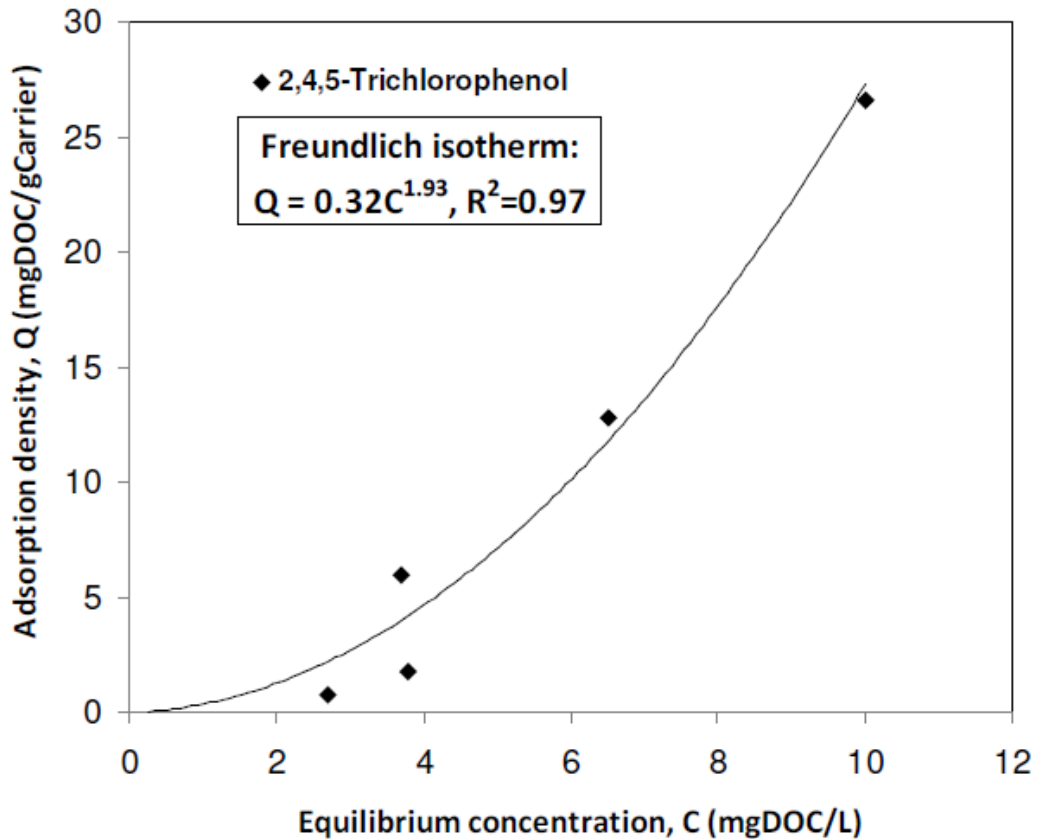


Figure 7. Equilibrium isotherm modeling of adsorption of TCP on the sponge carriers using the Freundlich isotherm. TCP mass is mg as DOC. The isotherm shows so-called “unfavorable” adsorption, or an exponent greater than 1.

ICPB in the PCBRR

In an ideal condition of intimate coupling, photocatalysis transforms biorecalcitrant contaminants into biodegradable intermediates that are immediately biodegraded and mineralized by microorganisms. Figure 8, which presents the results for the continuous operation of the PCBRR without and with biofilm in the carriers, demonstrates that the two steps of intimate coupling occurred when biofilm was present.

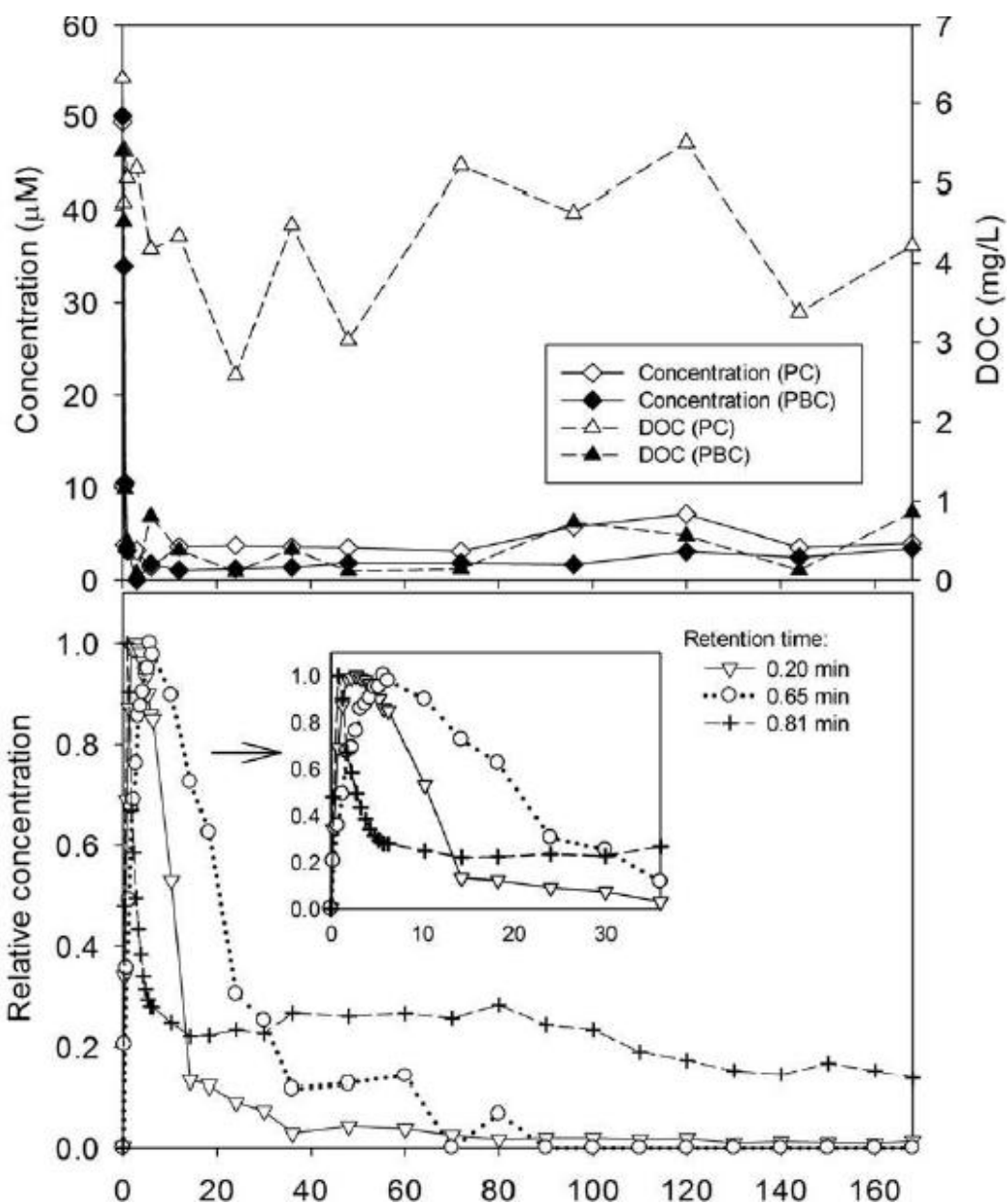


Figure 8. PCBRR operation results. The influent concentrations were 50 μM for TCP and 3.6 mg/L for DOC. 2,4,5-TCP and DOC concentrations for photocatalysis (PC) and photobiocatalysis (PBC) (Top). Relative concentrations of the three intermediates detected in the PBC experiments (Bottom).

Photocatalysis (combined with adsorption) removed approximately 93% of the TCP (from 50 μM to $\sim 3.5 \mu\text{M}$) from the liquid when the system reached steady state in the PC experiment. However, effluent DOC averaged around 4.3

mg/L, which was virtually the same as the influent DOC. When the carriers contained biofilm (the PBC experiment), TCP was removed to an even lower concentration, $1.9 \pm 1.0 \mu\text{M}$. Even more importantly, the effluent DOC was only $0.4 \pm 0.3 \text{ mg/L}$, or reduced by $\sim 90\%$ from the influent concentration. Thus, intermediates formed by photocatalysis were biodegradable, and mineralization was nearly complete. Mineralization was further confirmed by the release of $139 \pm 17 \mu\text{M Cl}^-$, which is 92% of the influent concentration of $150 \mu\text{M Cl}^-$ in TCP. In contrast to the previous cellulose carriers (Marsolek et al., 2008), we observed no material charring or loss of TiO_2 on the sponge carriers after the 7-days of operation in the PCBBR.

Patterns of Intermediates

We monitored the three major intermediates in ICPB of 2,4,5-TCP (shown in Figure 6c) over time. Since the chemical structures of the intermediates were not identified and thus had no standard curves for quantification, we computed relative concentrations from the peak areas of the UPLC chromatograms. The highest relative concentration of each intermediate was defined as “1,” and all other values were divided by the highest value to compute the relative concentrations (RC) shown in the bottom of Figure 8. All intermediates in the PBC experiment showed a similar trend: a rapid increase in the first 1 to 5 hours and then a decrease to a stable level by 15 to 40 hours.

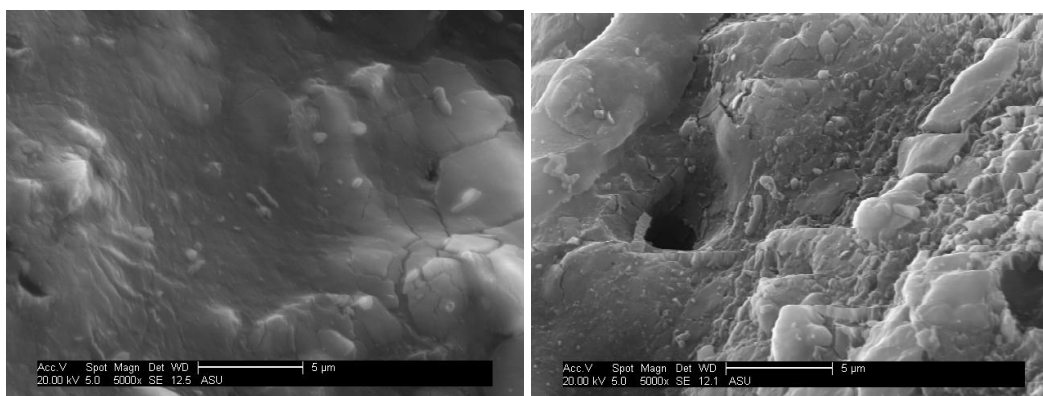
The intermediate at 0.18 min probably was the same product generated by photocatalysis, since the PC experiment had one peak at 0.18 min and that

behaved similarly to what is shown on Figure 8: the RC was reduced by 90% after 20 h operation and was maintained at a very low level after 40 h.

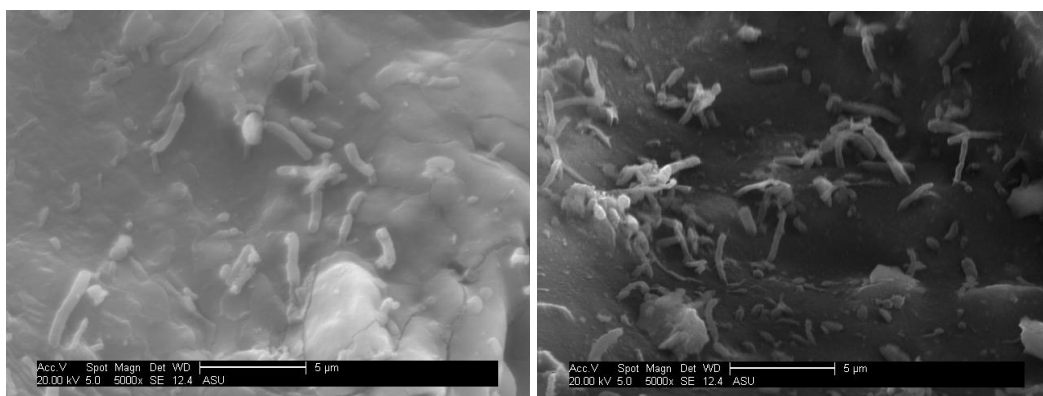
Presumably, the two other intermediates in the PBC experiment were generated from biodegradation, since they were not found in the PC experiment. The 0.65-min product showed the slowest production and consumption pattern, but achieved complete removal after 90 h. The fact that it increased at the time that the 0.18-min eluent declined suggests that the 0.65-min product may have been a biodegradation product of the 0.18-min eluent. In contrast, the peak at 0.81-min rose and fell even faster than 0.18-min product, and it stabilized after only 10 h operation, but with only around 80% removal. Perhaps it was generated by direct biodegradation of TCP and acted as the major component contributing to the DOC in the effluent of PBC experiment.

Biofilm during ICPB

Although microorganisms were dense on the exterior of the carrier immediately after cultivation (Figure 3), Figure 9a shows no microorganism on the outer surface of the carriers during and at the end of ICPB, although they clearly were present in the interior of the carriers (Figure 9b). This finding validates that biofilm formed in the interior was protected from the UV irradiation and hydroxyl free radicals, the objective of ICPB.



(a)



(b)

Figure 9. SEM images (5000X magnification) of exterior (a) and interior (b) of the sponge carriers after 48 h (left) and 240 h (right) operation in the PCBBR.

We also visualized microbial activity on the TiO₂-coated biofilm carriers by CLSM, as shown in Figure 10. Live cells grew in the carrier interior, while cells located close to the exterior were dead. Even for the interior of the carrier, the biofilm layer showed a gradient from live to dead, suggesting a self-sacrifice protection mechanism of biofilm when photocatalytic reactants invaded into the macropores. Additional evidence is provided by CTC staining of bacteria at the interior of the carrier, shown in Figure 10b. Metabolically active cells attached tightly along the wall of the macropore, while dead cells were clustered and appeared to hang loosely hung on the wall.

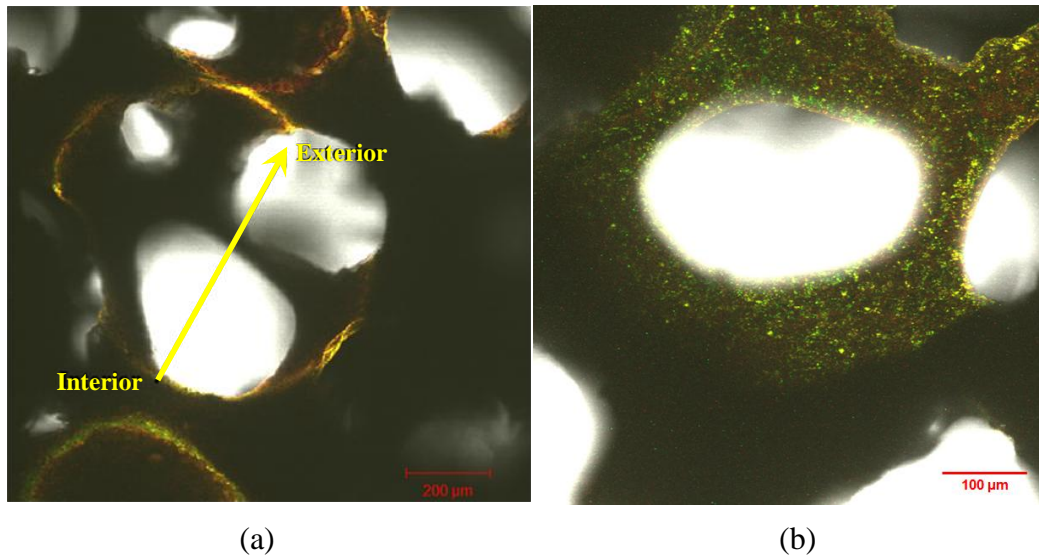


Figure 10. Merged CLSM images and light micrographs of the same region after live/dead staining (a) and CTC staining (b).

Pyrosequencing analysis of the microbial community

We used pyrosequencing to analyze the bacterial communities of the original inoculum (activated sludge), biofilm cultivated in the carriers, and biofilm enriched during ICPB. Figure 11 overviews bacterial diversity at the class level. The bacterial diversity showed little change between the activated sludge and the biofilm cultivated onto the carriers (25 or 27 classes, respectively), but ICPB significantly narrowed the community diversity to only 8 classes. All three communities were dominated by *Betaproteobacteria*, with the relative abundances of 67%, 65%, and 79%. The *Beta*, *Alpha*, and *Gamma* subdivisions of the *Proteobacteria* comprised more than 99% of community components after ICPB.

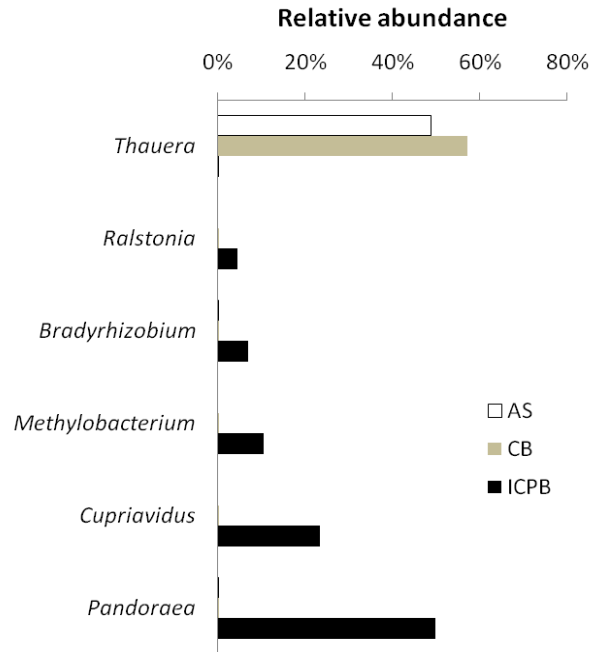
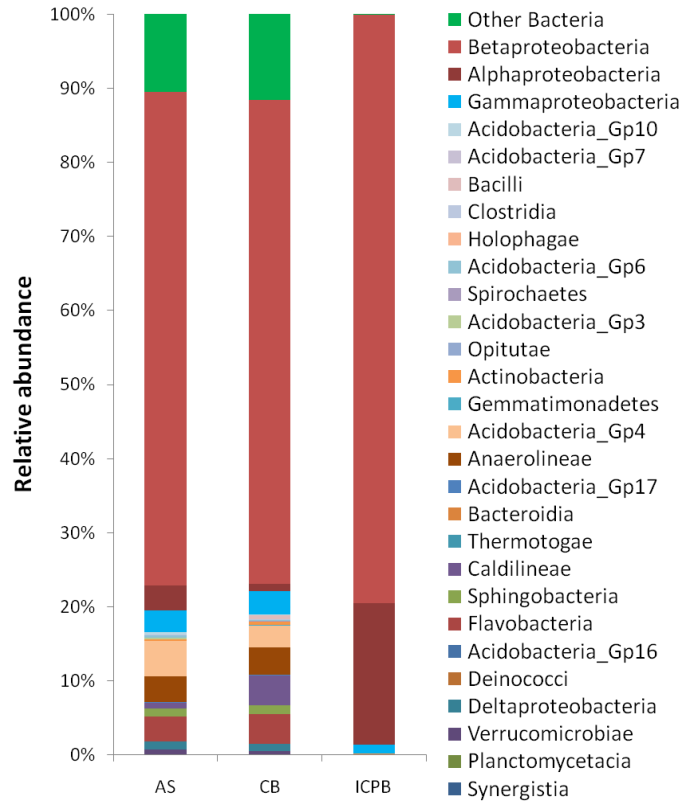


Figure 11. Pyrosequencing results from the activated sludge inoculum (AS), cultivated biofilm (CB), and after-operation sample (ICPB): (Top) Taxonomic breakdown at the class level and (bottom) predominant bacterial genera.

Figure 11 compares the community structures at the genus level on the bottom. Members of *Thauera*, a rod-shaped Gram-negative genus common to the activated sludge (Morgan-Sagastume et al., 2008; Mao et al., 2008; Zhang et al., 2011), were dominant in the biofilm cultivated on the carriers, but were almost completely eliminated after ICPB. In contrast, five genera that were undetectable or at very low abundance before ICPB -- *Ralstonia*, *Bradyrhizobium*, *Methylobacterium*, *Cupriavidus*, and *Pandoraea* -- were highly enriched on the carriers. Although each genus is known for its dechlorinating capability and/or degradation of chlorophenol derivatives (Steinle et al., 1998; Itoh et al., 2004; Adav et al., 2007; Jiang et al., 2009), none was reported to directly biodegrade 2,4,5-TCP. This suggests that they were biodegrading photocatalytic-degradation products of 2,4,5-TCP during ICPB.

Conclusions

This chapter demonstrated stable and efficient ICPB of 2,4,5-TCP in a continuous-flow PCBBR using a sponge-type, TiO₂-coated biofilm carrier. Compared to previous results, the carrier showed good performance in terms of TiO₂ adherence amount and strength, biomass cultivation, and resistance of oxidative charring. Among four possible TCP removal mechanisms, fast adsorption of TCP onto the sponge carriers dominated the early stage of removal and followed a Freundlich isotherm with an exponent close to 2. While photolysis gave no obvious removal of TCP, photocatalysis led to TCP primary break down. When biofilm was added to photocatalysis, TCP and the products of TCP photocatalysis were biodegraded and mineralized. Although UV light and hydroxyl free radicals killed the microorganisms on the outer surface of the carriers, biofilm was retained inside the macropores, which validated the premise of ICPB. The community after ICPB was substantially less diverse than the original inoculum and the cultivated biofilm before ICPB. The community was enriched in genres known for their capability to dechlorinate and biodegrade chlorophenol, which suggests that they mineralized photocatalytic products of 2,4,5-TCP degradation.

Chapter 3

DEGRADATION OF REACTIVE DYES IN A PHOTOCATALYTIC CIRCULATING-BED BIOFILM REACTOR²

Reactive dyes have been dominating the dye market for over a half century due to their advantages of low cost, simplifying the dyeing process, and improved fastness due to their reaction with cellulosic fibers (Freeman and Sokolowska, 1999; Bergamini et al., 2009). They are extensively used by textile, paper, and carpet industries, all of which generate large amounts of dye-containing wastewater that contains the unfixed residual dyes (Wang et al., 2009). Based on their characteristic strong colors, wastewater from the dyeing industries has become a major environmental concern in many countries (Nigam et al., 2000). Reactive dyes and their breakdown intermediates in the wastewater also can have direct toxicity to the aquatic organisms and can disrupt the photosynthesis process by reducing the penetration of the sunlight (Chung and Stevens, 1993; Won et al., 2008).

Typical reactive dyes consist of an azo-benzene chromophore attached to various types of reactive groups. The chromophores contain complex benzene units highly conjugated by azo-bonds (-N=N-), which adsorb visible light at specific wavelengths and produce colors from the reflected light (Carliell et al., 1995). The conjugation can be disrupted by destruction of the azo group, which causes decolorization of the reactive dyes (Beydilli et al., 2000).

² This chapter is adapted from a submitted paper: Degradation of Reactive Dyes in a Photocatalytic Circulating-Bed Biofilm Reactor. Li G and Rittmann BE. 2011. *Biotech. Bioeng.*

The reactive groups are made of haloheterocycles (e.g., dichlorotriazine) or activated double bonds derived from vinylsulfone or its ester (Steady, 1982; Renfrew, 1999). Combining two similar or different reactive groups, called homo- or hetero-bifunctional dyes, increases the fixation efficiency and minimizes dye wasting due to hydrolysis side reaction. Nonetheless, around 40% of reactive dyes are lost into the wastewater after the fixation process (Taylor, 2000).

The complex aromatic structures of reactive dyes, which make them resistant to color fading due to washing or light, also make them recalcitrant to biodegradation. Although biological treatment is preferred because of its low cost, energy saving, and extensive application in the wastewater treatment plants, it usually is not effective to remove reactive dyes from the wastewater (Kritikos et al., 2007). Several aerobic biological methods involving fungi and algae have been used to treat reactive dyes, but most of them decolorize the wastewater through adsorption rather than biodegradation. As a result, the dyes are not destroyed, but transferred to a solid phase (Mohan et al., 2002; Jadhav et al., 2007 and Daneshvar et al., 2007). Likewise, conventional physical-chemical treatments do not degrade the reactive dyes, but transfer them from one phase to another (Lee and Yoon, 2004). Anaerobic treatment has been shown to decolorize the reactive dyes by reduction of the azo group (Sponza and Işik, 2002). However, the aromatic-amine products can be even more toxic and mutagenic to aquatic living system than are the original reactive dyes, and the products also resist further degradation in anaerobic conditions (Mutambanengwe et al., 2007).

Recent studies have focused on advanced oxidation processes (AOPs) as an alternative based on the generation of free radicals, particularly hydroxyl radicals (OH), which are highly reactive towards a broad range of contaminants (Cho and Zoh, 2007). Decolorization of azo reactive dyes was reported with O_3/UV , $\text{H}_2\text{O}_2/\text{UV}$, $\text{Fe}^{2+}/\text{H}_2\text{O}_2$, and TiO_2/UV (Chen, 2000; Daneshvar et al., 2003&2004; Danion et al., 2004). Recently, Bergamini et al. (2009) reported that photocatalytic degradation of reactive dyes in aqueous TiO_2 suspensions could remove up to 97% of the color of a reactive dye bath, while others reported similar treatments to degrade reactive dyes, i.e., reactive black, orange, and red, which followed first-order kinetics (Genç 2004; Chatterjee, 2008). However, the subsequent removal of intermediates produced by the photocatalytic degradation of reactive dyes still need to be solved, particularly because it is economically infeasible to fully mineralize the reactive dyes with an AOP.

The novel Photocatalytic Circulating-Bed Biofilm Reactor (PCBBR), demonstrated by Marsolek et al. (2008), could be an ideal system to degrade and mineralize the reactive dyes. The PCBBR is a means to have photocatalysis and biodegradation (ICPB) occur simultaneously in one reactor. In ICPB, the reactive dyes are initially decolorized and broken down by photocatalysis on TiO_2 affixed to the outer surface of a macroporous carrier that also accumulates bacteria in its interior. The intermediates from photocatalysis are biodegraded and mineralized by the bacteria, which are protected from UV radiation, hydroxyl free radicals, and the toxicity of the reactive dyes and their intermediates by being inside the carrier.

We studied the photocatalysis step for three reactive dyes: Reactive Black 5 (RB5), Reactive Yellow 86 (RY86), and Reactive Red 120 (RR 120), whose structures and properties are given in Table 2. Based on those results, we investigated ICPB for RB5 using the PCBRR. We evaluated ICPB performance by the level of decolorization, extent of mineralization, effects on pH, and accumulation of bacteria in the carrier macropores. We also tracked the released ionic species and used this information to propose a degradation pathway of RB5 in the PCBRR.

Materials and Methods

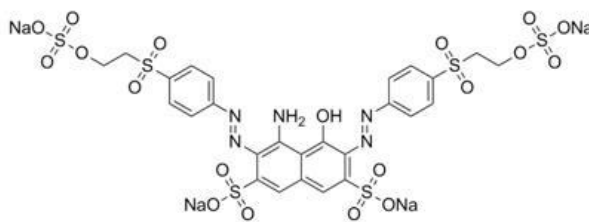
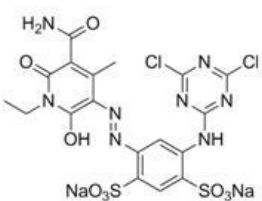
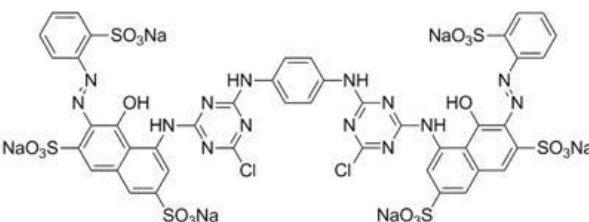
Materials

We purchased reactive dyes RB5 (55% dye content), RY86, and RR120 from Sigma-Aldrich (St. Louis, MO, USA) and used them without further treatment.

Table 2 summarizes the chemical structures, maximal absorption wavelengths, and number of azo-bonds and reactive groups for the three reactive dyes.

Table 2

Information on the reactive dyes

Name	Structure formulae	λ_{\max} (nm)	Reactive group
Reactive Black 5 (RB5)		600	Vinylsulfone (Diazo-dye)
Reactive Yellow 86 (RY86)		430	Dichlorotriazine (Azo-dye)
Reactive Red 120 (RR120)		520	Dichlorotriazine (Diazo-dye)

Standard solutions of SO_4^{2-} and NO_3^- were obtained from SpexCertiPrep, Inc. (Metuchen, NJ, USA). All other chemicals were of analytical grade. We

used the same macroporous sponge-type cubes, BioCAP® (Samsung Engineering Co., Ltd. Seoul, Korea), as the carrier in our PCBBR experiments.

Carrier Preparation

We coated photocatalyst titanium dioxide (TiO₂) onto the sponge-type carriers based on a modification of the sintering method we reported previously. We modified the procedure by reducing the concentration of suspended TiO₂ to 10% (from 13.2%) and removing the additive (trimesic acid), which we called “DN” method. The density of coated TiO₂ was 0.4 g/g carrier, and the coating efficiency after rising treatments was 80%. Compared to TiO₂-coated carrier used in chapter 2, the carriers coated by the modified method had a more even distribution that almost completely covered the outer surface of the carrier, and this significantly enhanced the decolorization efficiency with the reactive dyes. To make TiO₂-coated biofilm carriers, we inoculated activated sludge from the Northwest Water Reclamation Plant (Mesa, Arizona, USA) and cultivated it onto and into new TiO₂-coated carriers using the previous method.

Batch Experiments for Reactive-Dye Photocatalytic Degradation

We used TiO₂-coated carriers to compare the photocatalytic efficiency when degrading RB5, RY86, and RR120. We conducted degradation experiments in 100-mL beakers using 0.5 g TiO₂-coated carriers and 50 mL of 50- μ M reactive dyes solution. Each beaker was placed on a VWR 620 Standard Magnetic Stirrer (120V, 50/60Hz, 0.5A, 50W, Radnor, PA, USA), mixed with a 2-cm stir bar at room temperature (~25°C) under UV irradiation with irradiance of 2.0 mWatt/cm².

Liquid samples were taken at 0, 5, 10, 15, 20, 30, 45, 60 min and immediately filtered through 0.2- μm syringe filters before being measured by the spectrophotometer at the maximal absorption wavelength, shown in Table 2. We also measured chemical oxygen demand (COD) to monitor the extent of mineralization.

We investigated buffer interference on photocatalytic efficiency by using TiO_2 -coated carriers to degrade 40- μM RY86 in batch experiments. We used two 100-mL beakers, each containing 50 mL RY86 solution (40 μM); one beaker also had 10 mM phosphate buffer (pH = 7.0). We added 0.5 g carriers in each beaker and started the experiment with UV irradiation (2.0 mWatt/cm^2) after mixing carriers with the solution for 5 min. After one-hour of UV illumination, we immediately transferred the carriers into two separate beakers, both containing 50 mL RY86 solution (40 μM) without buffer for a second batch tests. We periodically acquired liquid samples to measure pH before filtration and RY86 concentration after filtration.

Photocatalytic Circulating-Bed Biofilm Reactor

We used the same bench-scale PCBRR and UV illumination as chapter 2. In brief, the 150-mL reactor was covered with aluminum foil, leaving 38% of total liquid volume on the riser side illuminated by two UV lamps with intensity as 3.0 mWatt/cm^2 . Carriers were circulated in the reactor by air-lift pumping. The influent was pumped into the reactor through a Masterflex L/S pump (Cole-Parmer, Vernon Hills, Illinois, USA) from a 10-L bottle filled with synthetic

medium consisting of 40 μM RB5 or RY86 and mineral components: 1.8 mM $(\text{NH}_4)\text{Cl}$, 45.0 μM CaCl_2 , 0.6 μM FeCl_3 , 4.2 μM $\text{MgCl}_2 \cdot 7\text{H}_2\text{O}$, 1.6 μM $\text{MnCl}_2 \cdot \text{H}_2\text{O}$, and 24.3 nM Na_2MoO_4 in MilliQ water (Marsolek et al., 2008). The influent was supplied at the rate of 0.4 mL/min, which provided a hydraulic retention time (HRT) of 6 h.

Sampling and Analytical Methods

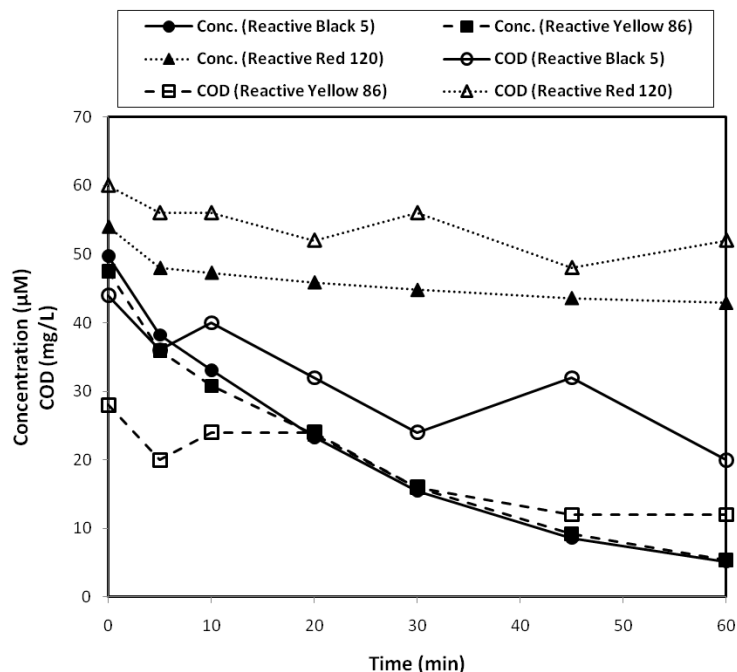
We collected liquid samples and carriers from the PCBBR by following the same procedures described previously. For the liquid samples, we measured pH with an Accumet® AB15 Basic pH/mV Benchtop Meter (Cole-Parmer, Vernon Hills, Illinois, USA) and then filtered the samples through a 0.2- μm PVDF membrane filter. The filtered samples were analyzed for concentrations of reactive dyes by a Cary 50 UV-Vis spectrophotometer (Varian, Inc., Sydney, Australia) at their maximal absorption wavelengths (λ_{max}), listed in Table 2. To assay mineralization, COD was measured by low range (3-150 mg/L) TNTplus™ Chemical Oxygen Demand Reagent from Hach Company (Loveland, Colorado, USA). SO_4^{2-} and NO_3^- were analyzed with an ion chromatograph (ICS-3000, Dionex, Sunnyvale, CA, USA) using a conductivity detector. We followed the same procedures to visualize microorganisms on the carriers by Scanning Electron Microscopy (SEM) using an XL30 environmental field emission SEM (FEI, Hillsboro, Oregon, USA).

Results and Discussion

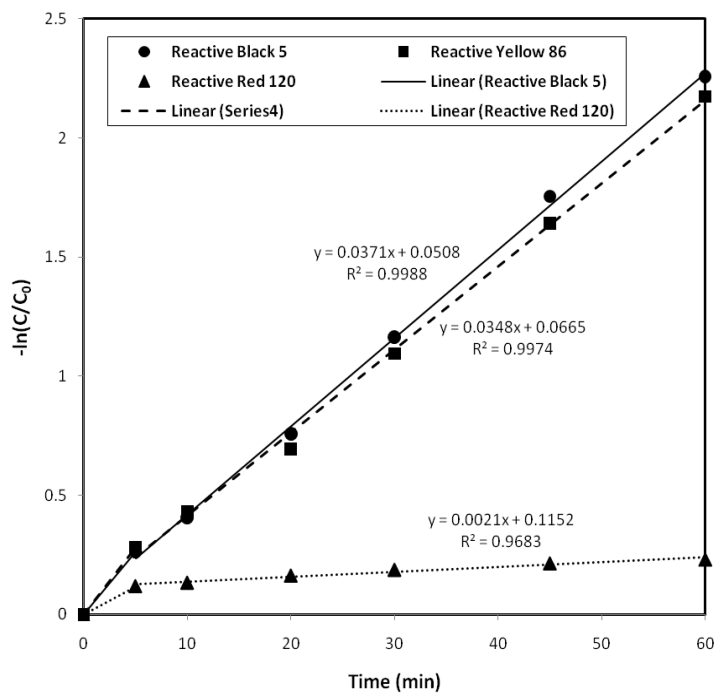
Decolorization Kinetics of RB5, RY86, and RR120

Figure 12a shows the results of batch experiments with TiO₂-coated carriers to investigate photocatalytic decolorization and mineralization of reactive dyes RB5, RY86, and RR120. RR120 showed a modest removal in the first 5 min, but minimal removal thereafter. This response indicates the RR120 was adsorbed on the sponge carriers, but had very slow photocatalytic degradation, probably due to its complex structure (Table 2). RB5 and RY86 also showed evidence of rapid adsorption, but then had sustained removals over the duration of the batch experiments. Figure 12b analyzes the reaction kinetics by a first-order model after the first 5 minutes (when adsorption dominated). RB5 and RY86 had almost the same first-order rates ($0.035 - 0.037 \text{ min}^{-1}$), about 17 times greater than for RR120.

Figure 12a also shows the fate of COD, which indicates if the dyes were mineralized. Loss of COD occurred in proportion to the adsorption of each reactive dye in the first five minutes. The COD continued to decline for RB5 and RY86, indicating that these molecules were transformed by the AOP. The removals of COD were less than the losses of the parent compounds: 55% versus 90% for RB5 and 57% versus 89% for RY86 after 1 h. Thus, both reactive dyes were only partially mineralized by the AOP.



(a)



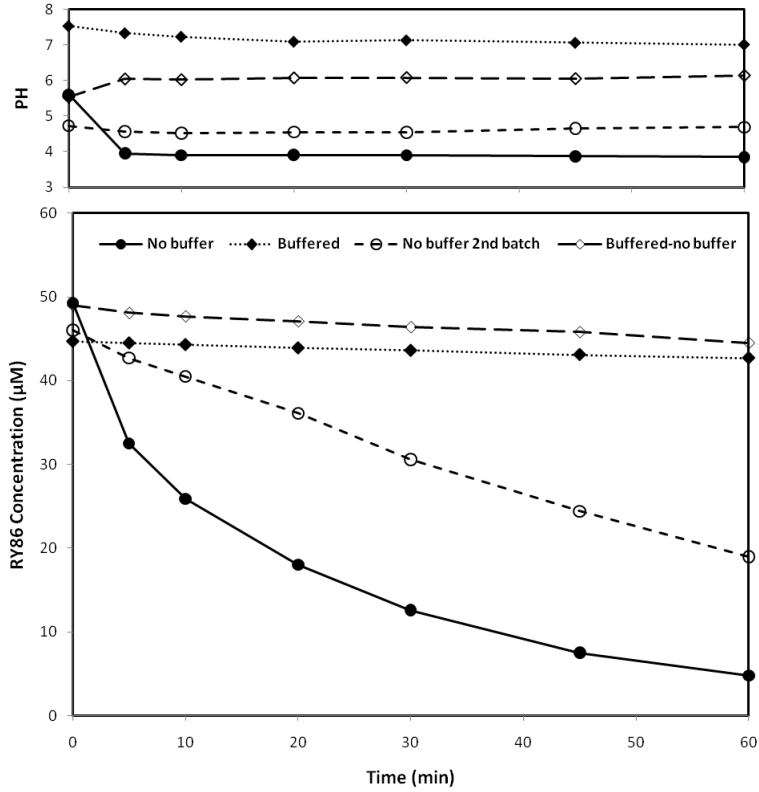
(b)

Figure 12. Adsorption and photocatalytic degradation of different dyes. (a) Reactive-dye concentrations and COD; (b) First-order kinetic model for reactive dye concentrations.

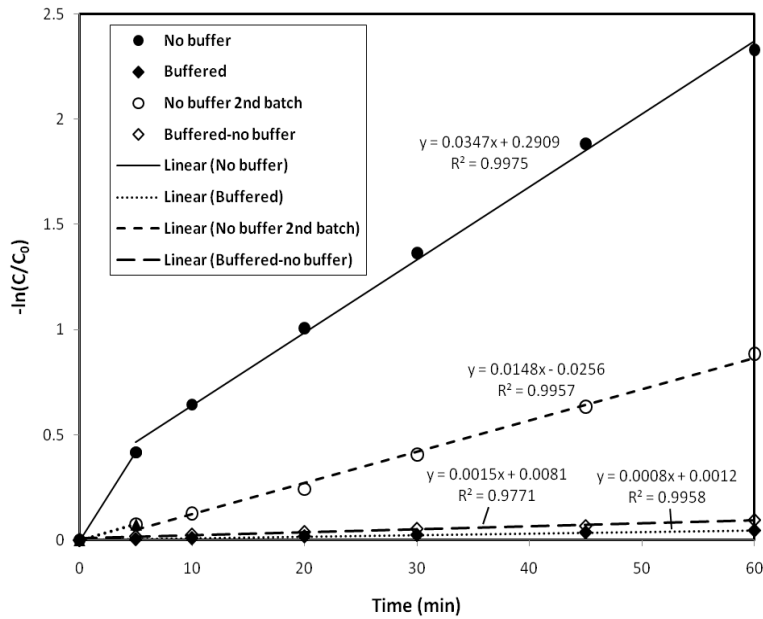
Degradation Interference by Buffering Additives

RB5 and RY86 solutions at 40-50 μM had acidic pH (~ 5), because the manufacturer acidified them for transportation and storage, as reactive dyes can be hydrolyzed under alkaline conditions (Weber and Stickney, 1993). Although it would be advantageous to adjust the solution pH closer to neutral (e.g., with a phosphate or carbonate buffer) to make conditions more favorable for biofilm growth, we found that addition of buffer inhibited the photocatalytic degradation of both reactive dyes. For example, Figure 13 shows that RY86 degradation was almost totally stopped at neutral pH achieved with a phosphate buffer. Furthermore, photocatalytic capability was not recovered when the TiO_2 -coated carriers were subsequently transferred into the original RY86 solution (no phosphate buffer). We obtained similar results of buffer inhibition with RB5 or by replacing phosphate buffer with carbonate buffer (Figure 14).

Degradation of reactive dyes is known to depend on the solution pH (Kritikos et al., 2007). A likely explanation of buffer inhibition in our experiment is related to the amphoteric character of TiO_2 , which is positively charged when $\text{pH} < 6.2$ and negatively charged if $\text{pH} > 6.2$ (Kritikos et al., 2007). Adsorption of the reactive dyes to the activated sites on the TiO_2 surface probably was the rate-limiting step for heterogeneous photocatalysis (Fujishima et al., 2008), and it would be impeded by charge repulsion from negatively charged TiO_2 surface when the pH is high enough to give it a negative charge.

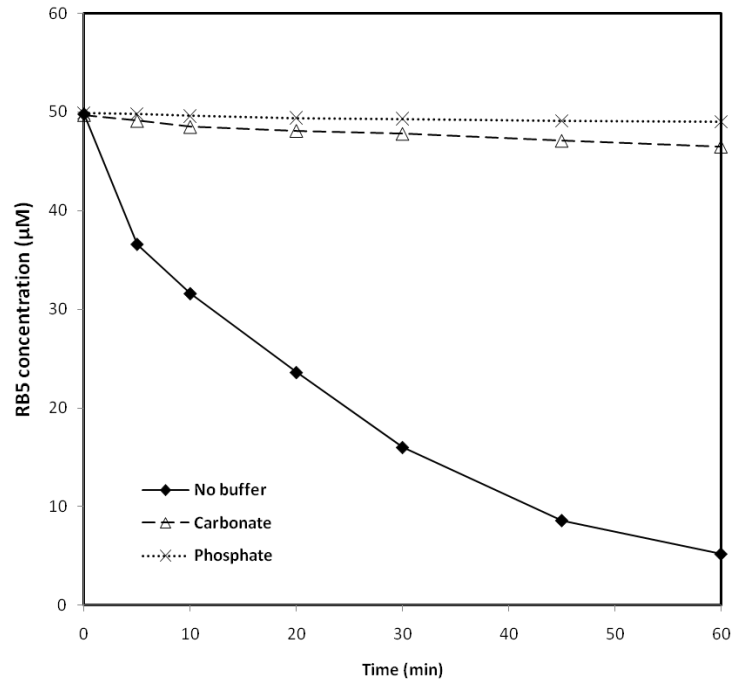


(a)

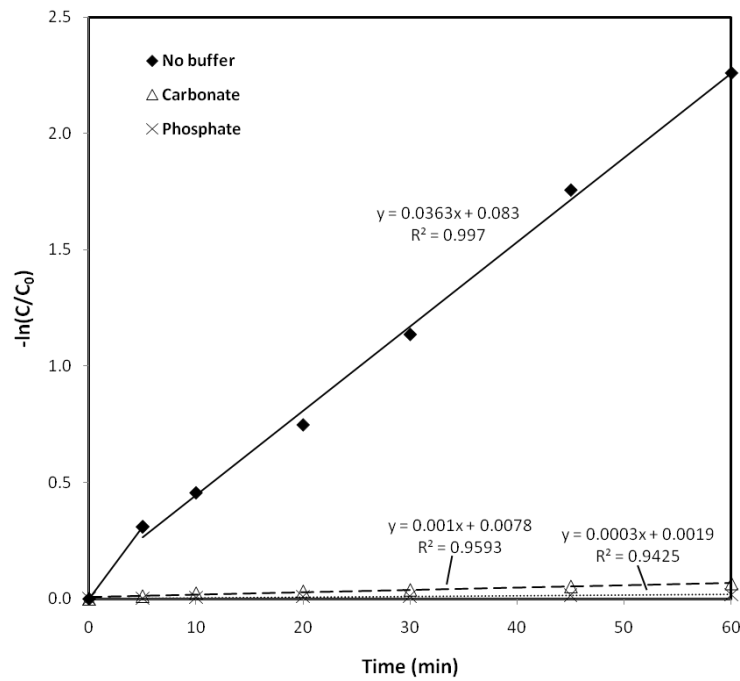


(b)

Figure 13. RY86 adsorption and photocatalytic degradation with or without phosphate buffer. (a) Concentration and pH; (b) First-order kinetic model.



(a)



(b)

Figure 14. RB5 adsorption and photocatalytic degradation with phosphate, carbonate, and no buffer. (a) Concentration; (b) First-order kinetic model.

The kinetics of photocatalytic surface reactions can be described by the Langmuir–Hinshelwood model (Roberts and Satterfield, 1965; Abdullah et al., 1990):

$$r = k(\Gamma_0 K_{eq} c) / (\Gamma_0 + K_{eq} c)$$

in which r is the reaction rate, k is the maximum reaction rate per adsorbed solute, Γ_0 is the maximum adsorption amount of the solute, K_{eq} is the adsorption equilibrium constant, and c is the reactive dye concentration in solution. Charge repulsion would decrease K_{eq} , and r would be reduced correspondingly.

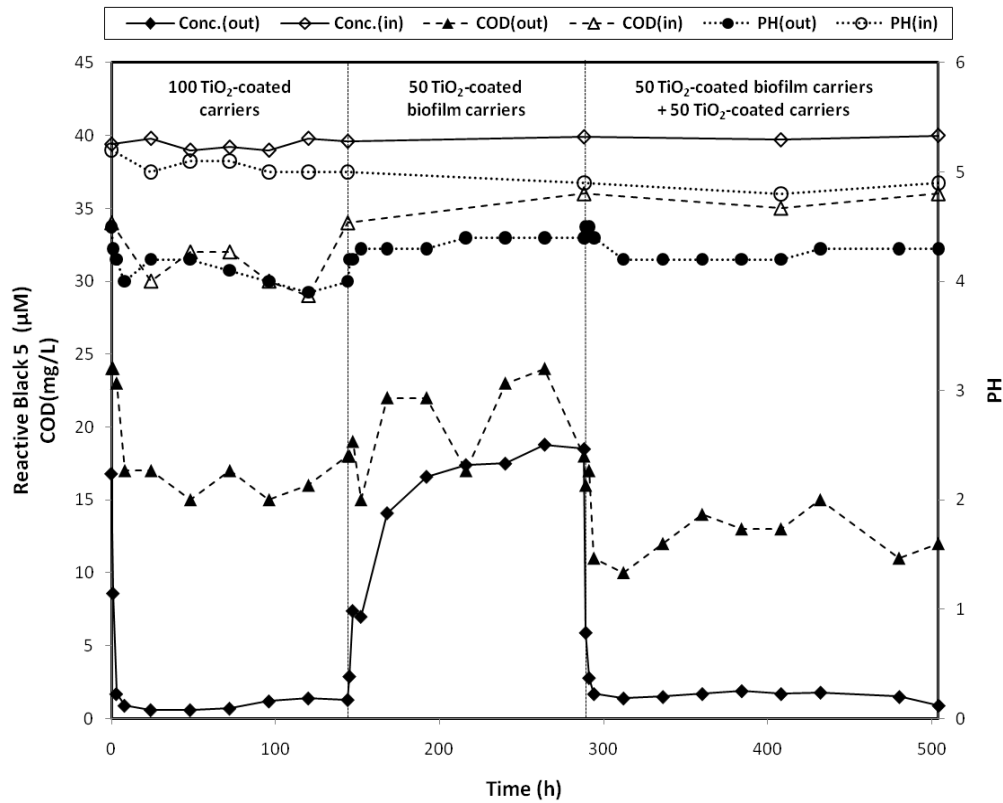
Regardless of the charge of TiO_2 , photocatalysis is known to be inhibited by strongly adsorbed anions, including phosphate and carbonate, which scavenge the photo-activated holes (h^+) or hydroxyl radicals (OH^\cdot) on the surface of TiO_2 , thereby slowing the photocatalytic degradation on organic substrates (Abdullah et al., 1990; Haarstrick et al., 1996; Bhatkhande et al., 2002). As the result, the photocatalytic reaction continued to be inhibited by adsorbed anions even after the pH was lowered to ~ 6 in the subsequent degradation experiment. To eliminate the problem of having very slow photocatalysis kinetics, we carried out the PCBBR experiments at low pH (~ 4.5) and without buffer.

Degradation of RB5 in the PCBBR

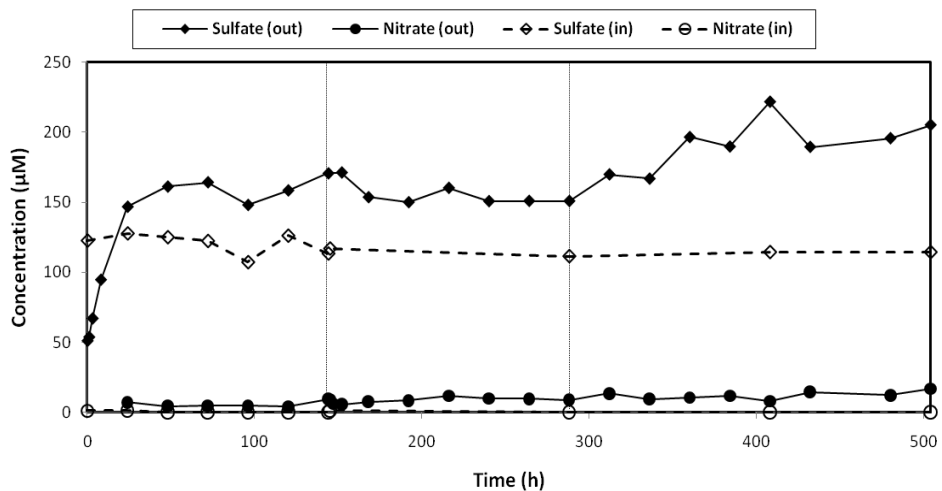
In order to evaluate ICPB of RB5 on the TiO_2 -coated biofilm carrier, we conducted PCBBR experiments in three stages. We first used 100 TiO_2 -coated carriers (no biofilm), then replaced those carriers with 50 TiO_2 -coated carriers also containing biofilm, and finally added 50 TiO_2 -coated carriers (no biofilm) to

enhance photocatalysis. Figure 15a compares the effluent and influent concentrations of RB5 and COD, as well as the pHs, for the three stages (the average of each stage is shown in Table 3). Photocatalysis alone removed 97% of the RB5, but only 47% of the COD. Thus, solely photocatalytic treatment of RB5 with 100 carriers achieved excellent decolorization, but failed to mineralize most of the photocatalytic intermediates. Exchanging 100 TiO₂-coated carriers with 50 carriers also containing biofilm led to only 57% removal of RB5, but COD removal declined only slightly, to 42%. Thus, decolorization efficiency was mainly tied to the amount of TiO₂, but the introduction of biofilm allowed significant biological mineralization of photocatalytic intermediates, as the fraction of decolorized RB5 that was further mineralized increased to 74%. Confirming these trends indicative of ICPB, RB5 removal recovered to 96% when 50 TiO₂-coated carriers were added, and COD removal was 65%.

ICPB was further proven by the release of N- and S-containing ions. While sulfite, nitrite, and ammonium had negligible changes in concentration (ammonium had a high influent concentration), Figure 15b shows that sulfate and nitrate increased after 25 min, and the increase grew as more COD removal occurred in the last stage. In the last stage, the increase in sulfate concentration was much larger ($86.8 \pm 12.2 \mu\text{M}$) than for nitrate ($12.2 \pm 3.1 \mu\text{M}$), which represent 66% and 11%, respectively, of the S and N originally in RB5. The generation of SO₄²⁻ reflects the mineralization of the SO₃-containing substituents around the aromatic core: i.e., R-O₂S-CH₂CH₂-SO₃⁻ and/or R-SO₃⁻, where R represents aromatic rings (see the structure in Table 2).



(a)



(b)

Figure 15. RB5 degradation experiments in the PCBBR. (a) RB5, COD, and pH. (b) Concentrations of sulfate and nitrate.

Carriers and Biofilm during ICPB

Due to the buffer and pH interference, we carried out the PCBRR experiments at low pH (~4.5), which normally has an adverse effect on the growth and metabolic activity of bacteria. One known exception is *Burkholderia* sp., which grew well while biodegrading naphthalene at pH 4 (to decrease cadmium toxicity) (Sandrin et al, 2002). Despite the low pH, Figure 16 shows considerable accumulation of bacteria inside of the biofilm carrier, and this is consistent with the significant mineralization seen in Fig. 15. Indicative of ICPB, the exterior of the carriers had much fewer bacteria (Fig. 16b). Thus, bacteria in the interior of the carriers were able to carry out the biodegradation function of intimate coupling despite the unfavorable pH environment needed to maintain strong photocatalysis.

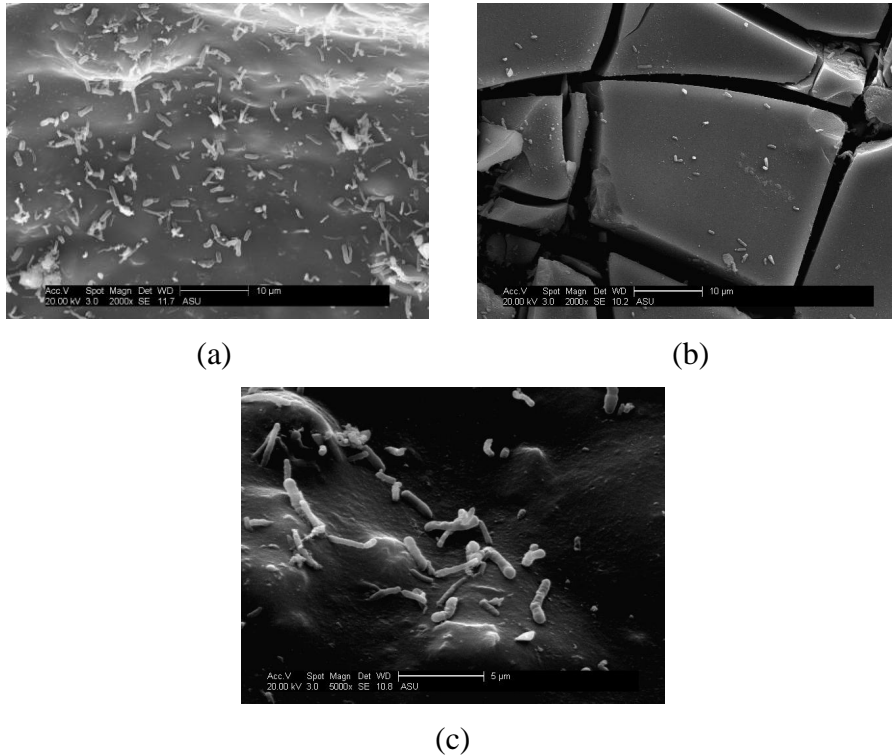


Figure 16. SEM images of carriers and harbored bacteria at the end of the RB5 experiment in the PCBRR. (a-b) Comparison of interior (a) and exterior (b) under 2000X magnification; (c) Interior under 5000X magnification.

Decolorization and Mineralization Pathway

According to the changes of RB5 and COD and large release of SO_4^{2-} ions, we propose in Figure 17 the likely pathway for most of the decolorization and mineralization of RB5 during ICPB. The organic C in RB5 contains 120 e⁻ equivalents, and RB5 also contains 6 equivalents of S and 5 equivalents of N (see Table 3). We track the fate of these equivalents at each step of the pathway in Table 4.

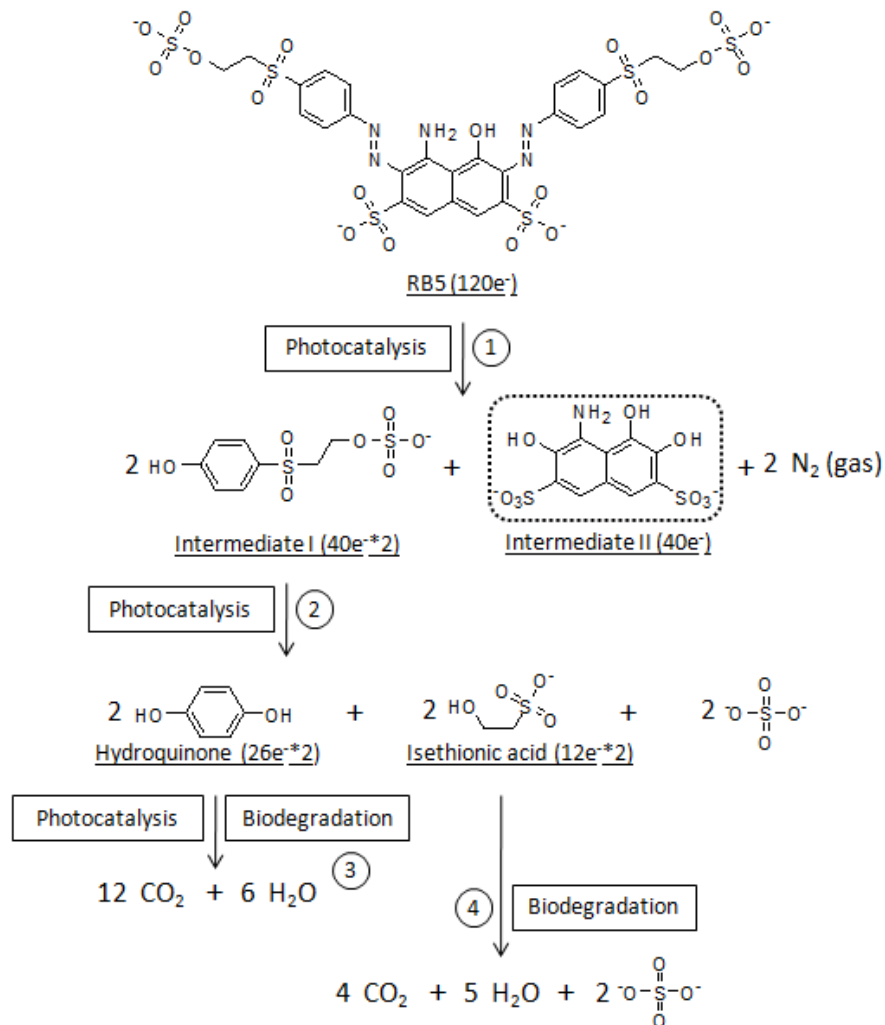


Figure 17. Proposed decolorization and mineralization pathway of RB5 by ICPB in the PCBRR. Each reaction step is labeled by a number, and its most likely mechanism is indicated.

Table 3

Comparison of effluent and influent concentrations during RB5 degradation

Stage	RB5 Concentration (μM)			COD (mg/L)		
	Effluent	Influent	Variation*	Effluent	Influent	Variation
I	1.2	39.4	38.2	16.6	31.2	14.6
II	17.2	39.9	22.8	21.0	36.0	15.0
III	1.6	39.9	38.3	12.3	35.5	23.2

Stage	Sulfate (μM)			Nitrate (μM)		
	Effluent	Influent	Variation	Effluent	Influent	Variation
I	159	120	39	6.2	0.2	6.0
II	155	117	38	8.8	1.2	7.5
III	200	113	87	12.2	0	12.2

Table 4

Equivalent balances for proposed ICPB pathway and comparison to experimental values.

Pathway step	COD removal e^- eq/mol RB5 (% of total)	Released sulfate mol S/mol RB5 (% of total)	Released N mol N/mol RB5 (% of total)
1	0 (0%)	0 (0%)	4 as N_2 (80%)
2	4 (3%)	0 (0%)	0 (0%)
3	52 (43%)	2 (33%)	0 (0%)
4	24 (20%)	2 (33%)	0 (0%)
1 + 2 + 3	56 (47%)	2 (33%)	4 as N_2 (80%) 0 as NO_3^- (0%)
Experimental PCBBR stage I (Photocatalysis)	56 (47%)	1.8 (30%)	0.27 as NO_3^- (5.4%)
1 + 2 + 3 + 4	80 (67%)	4 (67%)	4 as N_2 (80%) 0 as NO_3^- (0%)
Experimental PCBBR stage III (ICPB)	78 (65%)	4 (67%)	0.55 as NO_3^- (11%)

The first step is oxidative cleavage of the azo-bonds by hydroxyl radicals generated in photocatalysis, which has been reported through either C-N or N-N cleavage (Özen and Aviyente, 2003). Based on the low nitrite and nitrate detected in the effluent (Fig. 3b), photocatalysis oxidizes the azo-bonds mainly through C-N cleavages in the PCBBR, which brings about the release of di-nitrogen gas (N_2 , 80% of the total N in RB5) and the decolorization of the RB5 solution. Since C is not oxidized in this step, all $120 e^-$ equivalents are conserved in the step-one products: 2 moles of Intermediate I, a 2-(4-hydroxyphenylsulfonyl) ethyl sulfate, and one mole of Intermediate II, a naphthol derivative (4-amino-3,5,6-trihydroxynaphthalene-2,7-disulfonate). Based on residual COD (Fig. 15a) and incomplete release of S even with ICPB (Fig. 15b), we assume that Intermediate II remains undegraded and retains $40 e^-$ equivalents, 1 N equivalent, and 2 S equivalents, corresponding to 33% of the original COD, 20% of the N, and 33% of the S.

In the second step, the C-S bonds in intermediate I are cleaved by photocatalysis to release sulfate (2 moles S per mole RB5), isethionic acid (also called 2-hydroxyethanesulfonate, $HO-CH_2CH_2-SO_3^-$), and hydroquinone (also called 1,4-benzenediol). Together, isethionic acid and hydroquinone retain $24 + 52 = 76 e^-$ equivalents, or 63% of the original e^- equivalents in C. Step two also releases 33% of the original S equivalents, but no N. Summing steps one and two shows a loss of only 3.3% of the COD, release of 33% of the S as SO_4^{2-} , and release of 80% N as N_2 with the strictly photocatalytic reactions.

In step three, the hydroquinone is completely mineralized by either photocatalysis (Li et al, 1999) or biodegradation (Fava et al, 1995; Bae et al, 1996), which consumes 52 e⁻ equivalents, or 43% of the e- equivalents in the C of RB5. In step four, the isethionic acid is biologically mineralized to CO₂, SO₄²⁻, and H₂O. This consumes all of the COD and releases all of the N and S not contained in intermediate II.

When the PCBRR was operated in the strictly photocatalytic mode (the first stage), nearly 100% loss of RB5 resulted in the removal of 47% of the COD, and the S release as SO₄²⁻ was 1.8 mol S per mol RB5, or 30%. This correspondence between steps 1 – 3 of the pathway (Table 4: 47% COD removal and 33% release of S as SO₄²⁻) and the first stage of the experiments supports that step 3 probably occurred through photocatalysis.

When the PCBRR was operated with 96% removal of RB5 in the third stage, the COD removal was 65%, which corresponds well to steps 1 – 4 (67% COD removal). In this stage, the S release as SO₄²⁻ was 4.0 mol S per mol RB5, or 67%, which also corresponds well to the sum of steps 1 – 4 (Table 4: 66% S release as SO₄²⁻).

In first stage of PCBRR operation, N release as NO₃⁻ was 0.27 mol N per mol RB5, corresponding to only 5.4 % of the original N. In experimental stage three, N release as NO₃⁻ was 0.55 mol N per mol RB5, corresponding to 11 % of the original N. According to the pathway, 80% of the N is released as N₂ in step 1, while 20% is retained in Intermediate II. This small discrepancy with the

experimental results suggests that a degree of simultaneous N-N cleavage of azo-bonds occurred in parallel to in step 1, forming nitryl group (-NO₂) that was subsequently oxidized to NO₃⁻. Intermediate II and some of the biofilm on the carriers may also have been undergone a small amount of oxidative attack by photocatalysis, releasing NO₃⁻.

Conclusions

Reactive dyes RB5 and RY86 could be rapidly TiO₂-photocatalyzed at low pH (~4-5), but not at neutral pH (~7) maintained with a buffer (phosphate or carbonate). The inhibition probably was due to effect of pH on the surface charge of TiO₂, anion scavenging of radicals, or both. In the PCBBR, RB5 was nearly 100% decolorized by TiO₂-catalyzed photocatalysis, but the addition of biofilm substantially increased mineralization, which demonstrates that ICPB was occurring in the PCBBR despite a very low pH (~4.5) needed to prevent loss of photocatalytic activity. Further proof is the release of SO₄²⁻ and that bacteria were observed inside the carriers after the PCBBR experiments. Based on COD and S results, we propose a pathway for ICPB of RB5 in the PCBBR. Azo-bonds of RB5 are first oxidized to generate two intermediates and release N₂ gas through oxidative C-N cleavage. One intermediate, a naphthol derivative, remains undegraded, while the other is further photo-cleaved into two downstream-products: hydroquinone, which can be photocatalytically mineralized in the PCBBR, and isethionic acid, which is mineralized by the biofilm.

Chapter 4

DEVELOPMENT OF AN EFFICIENT TiO₂-COATED BIOFILM CARRIER FOR INTIMATE COUPLING OF PHOTOCATALYSIS AND BIODEGRADATION³

Intimate coupling of photocatalysis and biodegradation (ICPB) shows promise to remove recalcitrant organic compounds from water, because photocatalysis breaks the compounds into biodegradable intermediates that are immediately mineralized by microorganisms inside a macroporous carrier, where they are protected from UV light and free radicals. Key to successful ICPB is a carrier capable of accumulating biofilm in its interior and strongly adhering photocatalyst on its exterior.

In this chapter, we evaluated a commercially available macroporous sponge cube, BioCAP[®] (Samsung Engineering Co., Ltd. Seoul, Korea), as a new carrier for ICPB. As described in previous chapters, this sponge-type cube, made of polyurethane, has an average side length of 3.5 mm, which is good for sheltering biofilm inside while promoting photocatalysis on the outer surface. According to the manufacturer, this carrier has a high specific surface area of 4.8 m²/g by BET measurement, high porosity (88%), and a wet density close to that of water; all are appropriate for achieving sufficient adherence of TiO₂, accumulating biofilm, and giving good circulation in the reactor.

³ This chapter is adapted from a submitted paper: Developing an Efficient TiO₂-Coated Biofilm Carrier for Intimate Coupling of Photocatalysis and Biodegradation. Li G, Park S and Rittmann BE. (2011). *Appl. Catal. B-Environ.*

We explored a novel low-temperature (80 °C) sintering method (Cannon et al., 2005) to coat the sponge-type carrier with TiO₂. We then evaluated the coated carrier for its specific gravity for circulation, TiO₂ adherence and distribution, biomass accumulation, and performance in ICPB to degrade and mineralize 2,4,5-TCP. We further developed two improved coating methods, called the D and DN methods, to improve photocatalytic efficiency for degrading complex organic compounds, e.g., reactive dyes.

Materials and Methods

Chemicals

We purchased 2,4,5-trichlorophenol (98%) and Reactive Black 5 (RB5) from Sigma-Aldrich Company (St. Louis, MO, USA) and Titanium (IV) isopropoxide (97+%) and 1,3,5-benzenetricarboxylic acid (trimesic acid, 98%) from Alfa Aesar Company (Ward Hill, MA, USA). All other chemicals used in the experiments were of analytical grade.

TiO₂-coating procedure

We coated titanium dioxide (TiO₂) photocatalyst onto the sponge-type carriers according to a low temperature sintering method, described in chapter 2, called the O method, which stands for “original.” In an attempt to improve the photocatalytic efficiency of coated TiO₂, we modified the O procedure by reducing the TiO₂ concentration of the suspended coating solution; we call this the D method for “diluted.” We then removed the additive (trimesic acid) from the coating solution of the diluted process, creating the DN method for “diluted and no additive.” The detailed conditions for each method are summarized in Table 5. The density of coated TiO₂ was 0.5, 0.44, and 0.4 g/g carrier, and the coating efficiency after rising treatments was 75%, 88%, and 80% for the O, D, and DN methods, respectively.

Table 5

Comparison of the coating procedures

Procedure	O	D	DN
Nitric acid (0.075N)	150 mL	150 mL	150 mL
Titanium isopropoxide	23.9 g	23.9 g	23.9 g
Volume after evaporation	50 ml	67 ml	67 ml
Additive (trimesic acid)	5%	5%	0%
Coating solution/1 g carrier	5 mL	5 mL	5 mL
Theoretical weight	1.67 g	1.50 g	1.50 g
Actual weight after rising	1.50 g	1.44 g	1.40 g

O = original; D = Diluted; and DN = Diluted and No additive.

Reactive Black 5 (RB5) degradation experiments

We conducted RB5 degradation experiments in 250-mL beakers to evaluate photocatalytic efficiency of TiO₂-coated carriers prepared with the three coating methods, i.e. O, D, and DN. Each beaker contained 100 mL 40- μ M RB5 solution and 1.0 g TiO₂-coated carriers. Each beaker was placed on a VWR 620 Standard Magnetic Stirrer (120V, 50/60Hz, 0.5A, 50W, Radnor, PA, USA), mixed with a 2-cm stir bar at room temperature (~25°C) and under UV irradiation with a light intensity of 3.0 mWatt/cm². Liquid samples were taken periodically (i.e., 0, 5, 10, 15, 20, 30, 45, 60 min) and filtered through 0.2- μ m syringe filters before being measured by a Cary 50 UV-Vis spectrophotometer (Varian, Inc., Sydney, Australia) at the maximal absorption wavelength of RB5 (600 nm).

Results and Discussion

TiO₂-coating and biofilm cultivation

The left part of Figure 18 shows an uncoated sponge-type cube; it had a black color, a macroporous structure, and a wet density of 1.01 – 1.02 g/cm³, which allowed good circulation in the PCBBR. The right part of Figure 18 shows that the outer surface of the carrier turned grey due to attachment of TiO₂ particles after the O sintering method. The TiO₂ density was approximately 0.5 g/g based on dry-weight increase. This is 7 times greater than the 0.06 g/g density that Marsolek et al. (2008) achieved for the cellulosic carrier with a sol-gel method.



Figure 18. Sponge-type carrier before (left) and after (right) TiO₂ coating by the O method. The color of sponge-type carrier originally was black, but it changed to grey due to TiO₂ coated on the outer surface.

According to the SEM images of the uncoated sponge carrier and the TiO₂-coated carrier, shown respectively in Figures 19a and 19b, small blocks of coated material (100-200 μm in length) were scattered over the surface of the coated sponge carrier. Elemental mapping of the carrier surface by EDS showed that the small blocks deposited on the uncoated carrier were composed of TiO₂ (green signal dots in Fig. 19b). Quantitative analysis of the elemental distribution

on the carrier in Figure 20 provides further proof of good adherence of TiO_2 on the carrier surface.

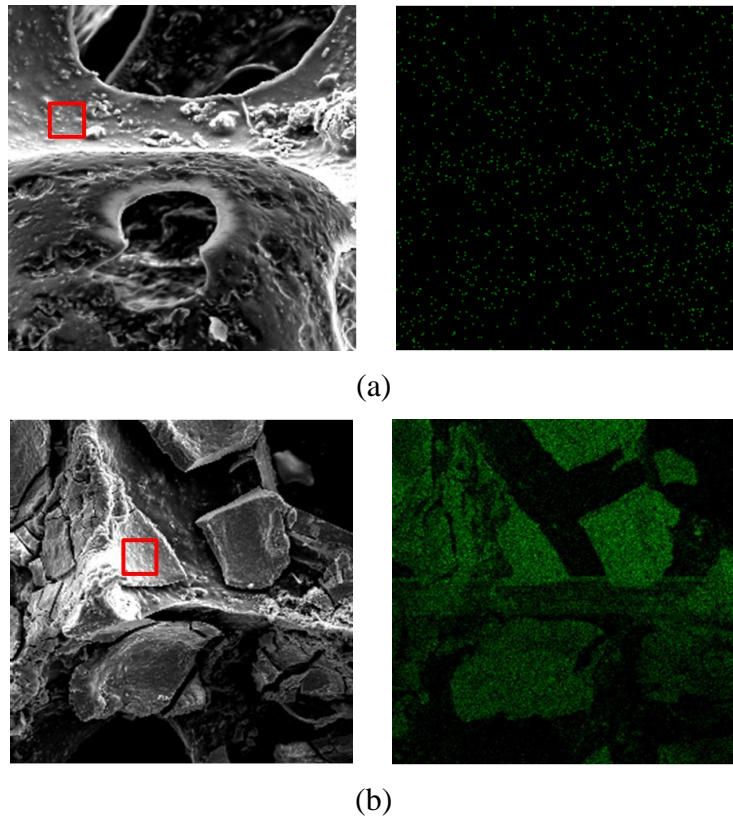


Figure 19. SEM images of the carriers under 200X magnification (left) and EDS elemental mapping (right) of uncoated carrier (a) and TiO_2 -coated carrier by the O method (b). The distribution of titanium is shown by green dots in the EDS elemental maps.

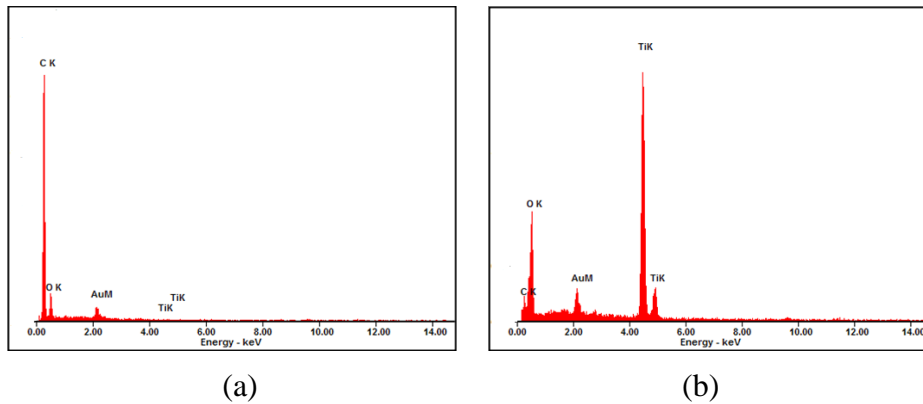


Figure 20. Elemental analysis by EDS of selected regions (red squares in Figure 19) on uncoated carrier (a) and TiO_2 -coated carrier by the O method (b). The element represented by each peak is labeled above the peak.

Figure 21a shows a cross-section SEM image of a cut TiO₂-coated carrier after biofilm cultivation. TiO₂ was restricted to the outer surface of the carrier with the O method, enhancing the photocatalytic efficiency of the adhered TiO₂ and presumably leaving the interior clear for biofilm growth (labeled by red dotted circle). Compared to an uncoated carrier, the macropore structure of the sponge-type carrier was unaffected by coated TiO₂, which is beneficial for microorganism migration inside to form biofilm. Figures 21b and 21c exhibit that microorganisms successfully accumulated in the interior of the carrier and without loss of coated TiO₂ on the outer surface.

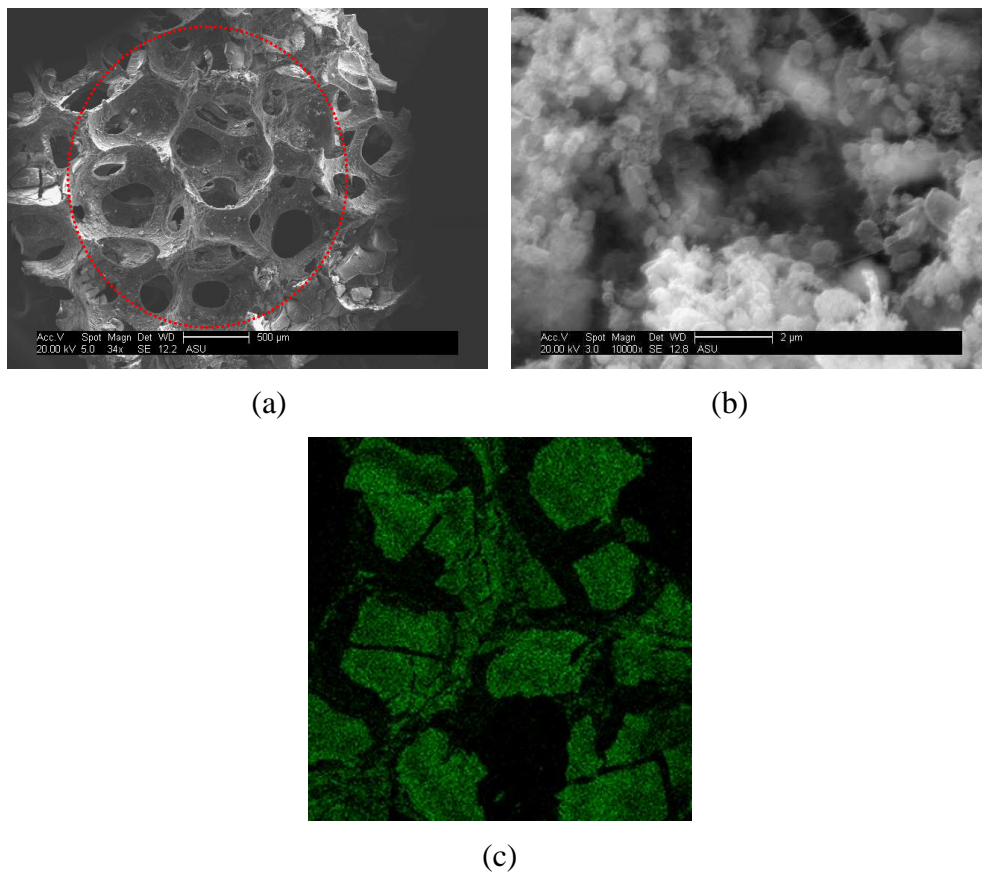


Figure 21. SEM images of middle section of TiO₂-coated biofilm carrier (34X, O method) (a) and cultivated bacteria (10000X) on the carrier (b); (c) Elemental mapping of TiO₂-coated carrier after cultivation by EDS (200X).

ICPB of 2,4,5-TCP in the PCBRR

We already reported that we could achieve stable ICPB for degrading and mineralizing 2,4,5-TCP using the biofilm carriers coated with TiO₂ by the O-method describe in chapter 2. In a comparable operating period in the PCBRR (~7 days), the O-method carriers overcame the obstacles reported by Marsolek et al. (2008): oxidative charring of carriers and insufficient adherence of TiO₂. The pH was stable between 6 and 7 during the operation, which was sufficient for biomass growth to achieve ICPB. Here, we provide additional information on the carriers at the end of 34 days of continuous operation of the PCBRR for TCP degradation, following the same procedure described above in chapter 2.

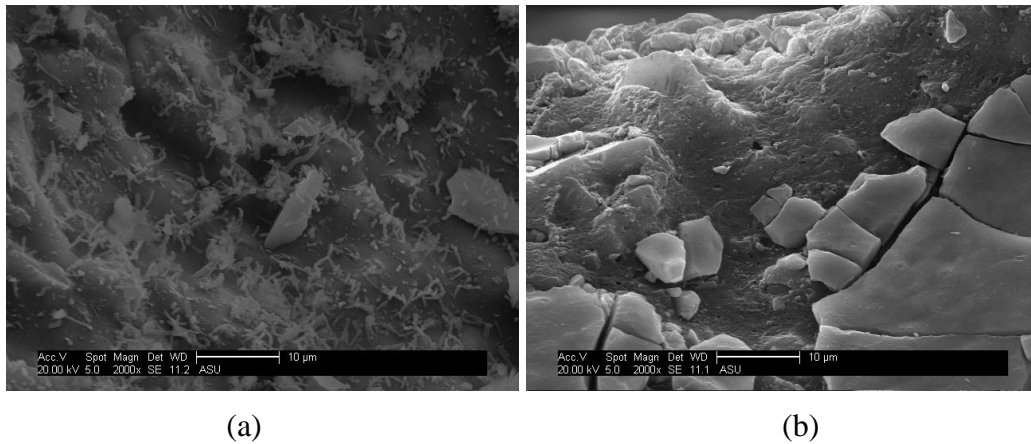


Figure 22. SEM images of interior (a) and exterior (b) of TiO₂-coated biofilm carrier (O method) after degrading 2,4,5-TCP after 34 days in the PCBRR.

Figure 22a proves that the accumulation of microorganisms was substantial inside the carriers, but few bacteria remained on the outer surface after 34 days. Figure 22b shows that some TiO₂ was lost from the carrier surface over 34 days, but SEM and EDS images of TiO₂-coated carriers after 34 days,

presented in Figure 23, continued to detect TiO_2 on the outer surface of carrier. Therefore, the sponge-type carriers coated with TiO_2 by the O method were superior to the cellulosic carriers of Marsolek et al. (2008) and met our basic requirements for ICPB and circulation in the PCBBR degrading 2,4,5-TCP.

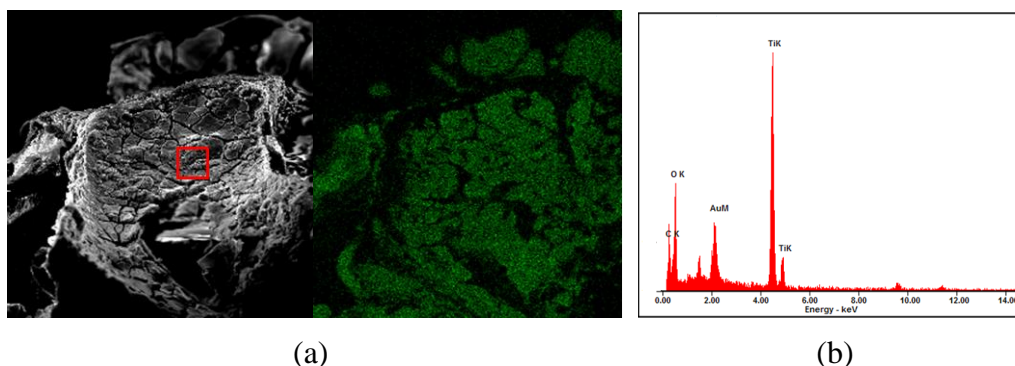


Figure 23. SEM image (left) and elemental mapping by EDS (right) of biofilm carrier coated with TiO_2 (O method) after TCP degradation experiment in the PCBBR.

Improved TiO_2 coating pattern and enhanced photocatalytic efficiency

Although TiO_2 -coating by the O method succeeded for the relatively simple aromatic compound 2,4,5-TCP, we found it exhibited relatively slow kinetics for organic contaminants with more complex structures, such as reactive dyes; we show an example of this experimental finding later (Figure 27). The large blocks of TiO_2 , may reduce the number of active TiO_2 -catalysis sites, since most of them are hidden inside the blocks, while bare carrier surfaces remain exposed (shown in Figure 19b). This underscores the importance of an improved TiO_2 -coating method that can form a thinner TiO_2 layer having more uniform coverage of the outer surface of the carriers. Therefore, we sought an improved sintering method

that would utilize the TiO_2 more efficiently and also protect the sponge material from UV irradiation.

Figure 24 shows that carriers coated with TiO_2 by the D and DN methods produced thinner catalyst layers and a more even distribution that almost completely covered the outer surface of the carrier. The macropore structure continued to be conserved. The layer coating by TiO_2 was confirmed by elemental mapping of the carrier surface in Figure 25. Comparing the D and DN coating patterns with higher magnification in Figure 26, it is clear that DN had better surface coverage than D.

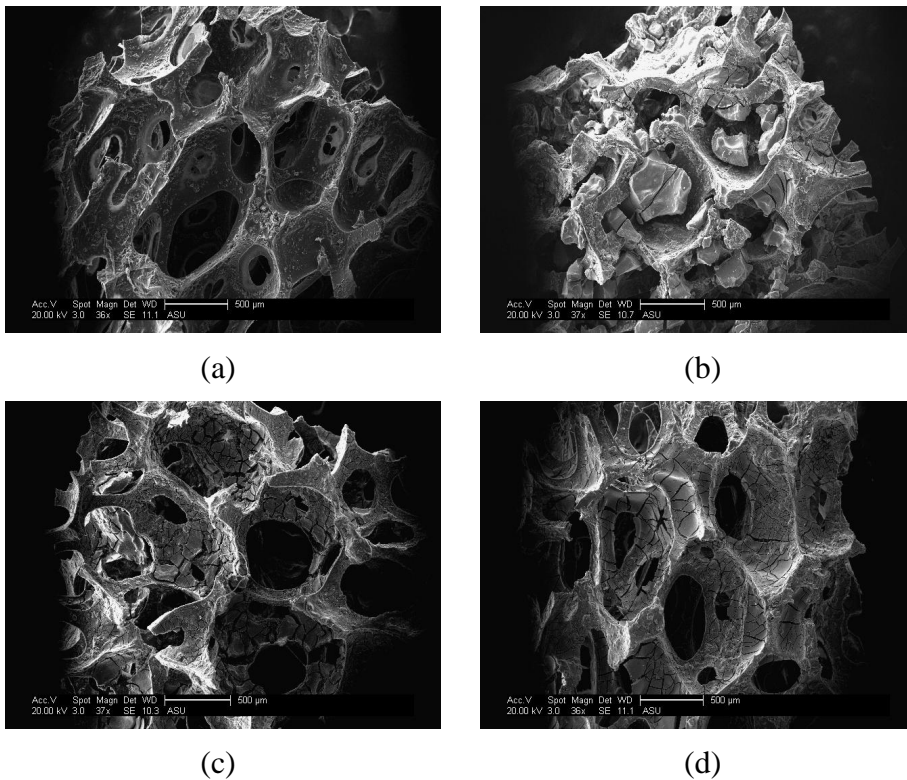
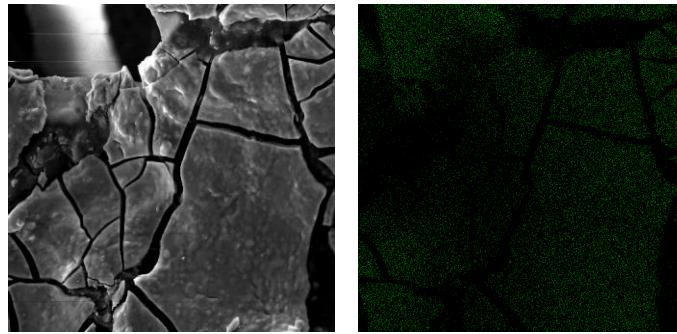
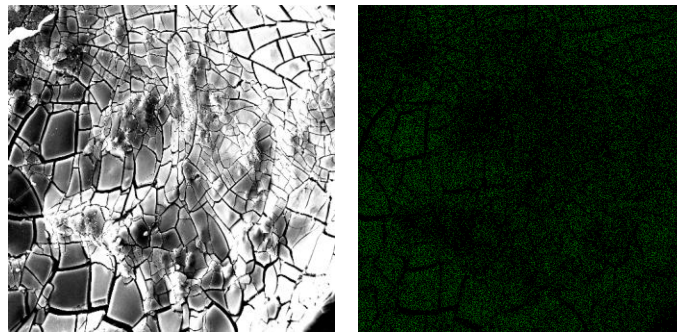


Figure 24. SEM images of uncoated carrier (a) and TiO_2 -coated carriers with O (b), D (c), and DN (d) methods at 36-37X magnification.

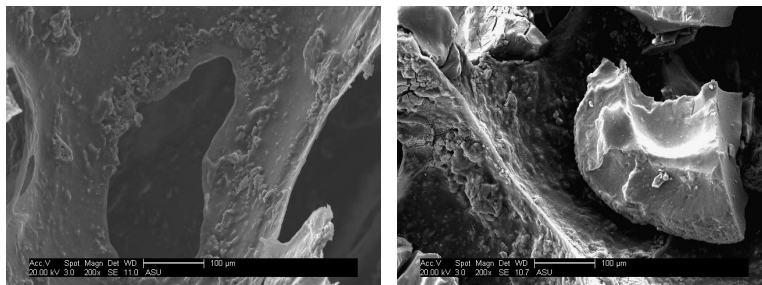


(a)



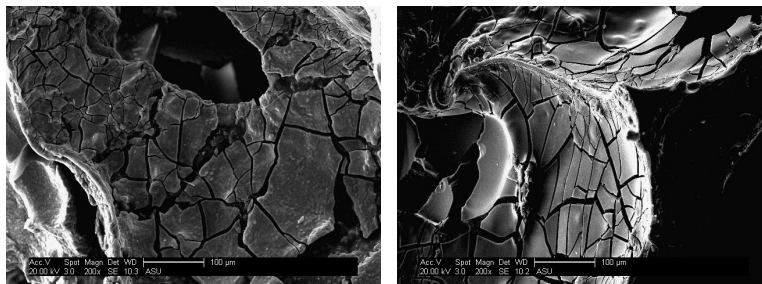
(b)

Figure 25. SEM image (left) and titanium mapping by EDS (right) of TiO_2 -coated carriers with D method (a) and DN method (b).



(a)

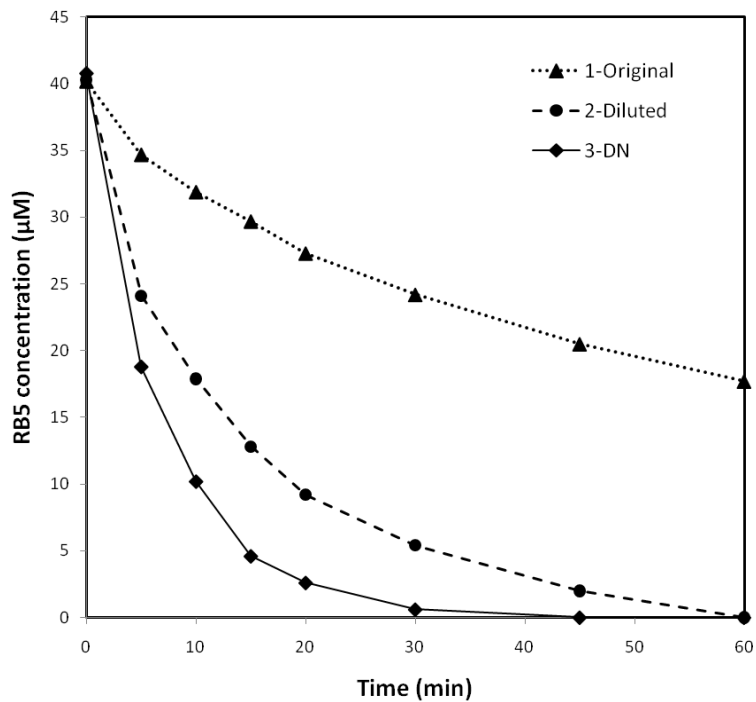
(b)



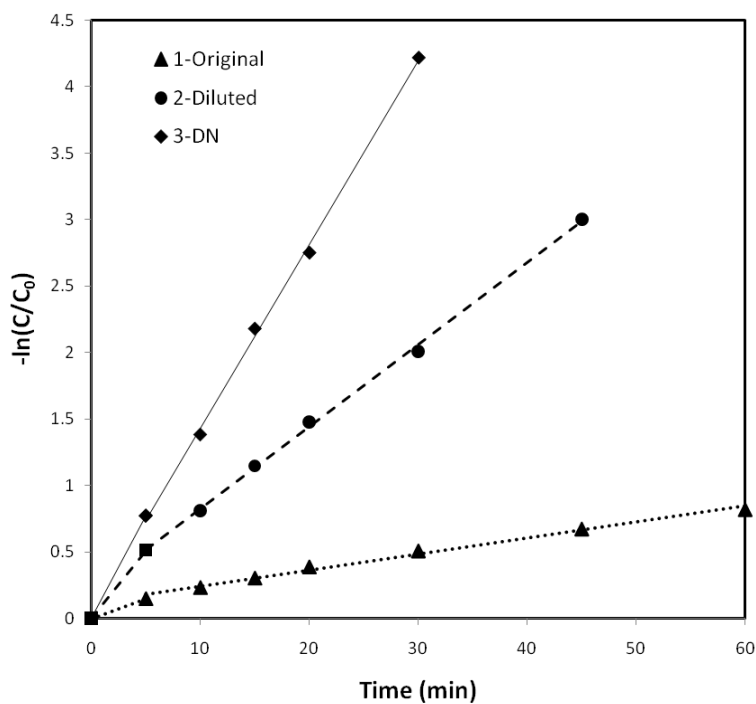
(c)

(d)

Figure 26. SEM images of uncoated carrier (a) and TiO_2 -coated carriers with O (b), D (c), and DN (d) methods at 200X magnification.



(a)



(b)

Figure 27. RB5 adsorption and photocatalytic degradation using TiO_2 -coated carriers prepared with the three different coating procedures (listed in Table 5). (a) RB5 concentration; (b) First-order kinetic model for RB5 degradation.

Figure 27 shows photocatalytic decolorization of RB5 in batch experiments using the TiO₂-coated carriers by the O, D, and DN methods. Adsorption and photocatalysis contributed to RB5 removal in the first 5 min, and sustained photocatalytic decolorization took place thereafter, following first-order kinetics, as our previous studies reported (Genç 2008; Chatterjee et al., 2008). Since uncoated carriers showed no adsorption of reactive dyes, adsorption was caused by the coating components, most likely TiO₂. Table 6 shows that the DN carrier gave the most enhanced photocatalytic activity (10 times that of the O carrier), while the D method increased photocatalytic efficiency by 5 times of the O carrier.

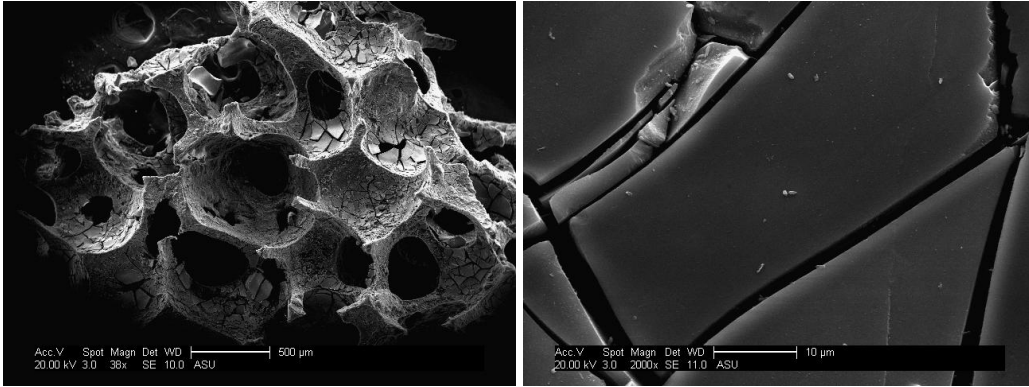
Table 6

First-order kinetic constants for RB5 photocatalytic degradation using carriers with the three sintering-based coating procedures

Coating method	Kinetic constant stage II (min ⁻¹)	R ²
O	0.012	0.991
D	0.062	0.999
DN	0.138	0.998

Stage II is from 5 minutes to 60 minutes, which is after initial adsorption.

Figure 28 shows SEM images of the DN-coated biofilm carrier operated in the PCBBR for 30 days for degrading RB5. It exhibited no obvious loss of coated TiO₂, suggesting that the DN method was superior to the O method in terms of adherence of the catalyst, resistance to abrasion, or both.



(a)

(b)

Figure 28. SEM images of biofilm carriers coated with TiO₂ by the DN method after ~30-day PCBBR operation for degrading RB5.

Conclusions

In this chapter, we evaluated a low-temperature sintering method, the O method, to adhere TiO₂ to sponge-type macroporous carriers. The O method achieved a 7-fold increase of TiO₂ density, compared to the previously used sol-gel method, and it conserved the macropores for biofilm accumulation. Although the O-method carrier met the basic requirements of ICPB when degrading 2,4,5-trichlorophenol, it had low photocatalytic activity for breaking down more complex aromatics, like reactive dyes. Therefore, we improved the sintering method in two steps called the D and DN methods: reducing the TiO₂ concentration and then removing trimesic acid in the coating solution. The photocatalytic efficiency towards reactive black 5 increased 5 fold for the D method and 10 times for DN method, and the DN carrier had superior TiO₂ adherence during long-term operation.

Chapter 5

OVERALL CONCLUSIONS AND RECOMMENDATIONS

This work demonstrates the viability of using a novel sponge-type, TiO₂-coated biofilm carrier to bring about ICPB for degrading and mineralizing two types of recalcitrant organic compounds in the PCBBR: 2,4,5-TCP and RB5. Reducing the TiO₂ concentration and removing the additive (trimesic acid) during low-temperature sintering produced a thinner and more uniform TiO₂ coating pattern, and this led to superior photocatalytic efficiency and adherence strength.

For 2,4,5-trichlorophenol, ICPB in the PCBBR achieved complete mineralization of the contaminant on the carrier. The carrier showed strong TCP adsorption, which enhanced biodegradation by relieving toxicity, and it allowed good accumulation of biofilm in its interior, where they were protected from UV light and free radicals. ICPB also showed a strong impact on the microbial community structure: reducing its diversity and selecting for chlorinated phenol-degrading genera, including *Ralstonia*, *Bradyrhizobium*, *Methylobacterium*, *Cupriavidus*, and *Pandoraea*.

For RB5, a contaminant even more complex and recalcitrant than TCP, the best TiO₂-coated (DN) carrier could almost completely remove RB5 and allow ICPB despite a low pH. Tracking the concentrations of RD5, COD, N, and S made it possible to propose a pathway for ICPB of RB5 in the PCBBR. Photocatalysis broke RB5 into 4-amino-3,5,6-trihydroxynaphthalene-2,7-disulfonate, isethionic acid, and hydroquinone, which released 80% of RB5's N as

N₂ and 33% of its S as sulfate. Biodegradation brought about complete mineralization of isethionic acid and hydroquinone into CO₂, SO₄²⁻ (33% of the S), and H₂O, and this allowed 65% COD removal in the total ICPB process. One initial photocatalysis product, a naphthol derivative, was resistant to further photocatalysis and biodegradation, and it retained 35% of the COD, 20% of the N, and 33% of the S.

Because the sponge-type carrier gave promising results, we should continue investigating and optimizing the fundamental parameters affecting PCBBR performance: e.g., temperature, pH, UV intensity, TiO₂ coating, and hydraulic retention time. We also should explore other types of biorecalcitrant organics, such as energetics and pharmaceuticals. This information will make it possible to maximize the efficiency of ICPB for degrading and mineralizing a range of recalcitrant and toxic organics. Further studies also should compare the composition of microbial community inside the carrier at different operating conditions for ICPB and when applying different contaminants in the PCBBR. Finally, interpreting the experimental data with numerical modeling of the PCBBR will link the reactions and gain mechanistic understanding of ICPB so that we can reliably understand and predict the fates of biomass, the target compound, and intermediates in the PCBBR.

REFERENCES

- Abdullah, M.; Low, G.K.C.; Matthews, R.W., 1990. Effects of common inorganic anions on rates of photocatalytic oxidation of organic carbon over illuminated titanium dioxide. *J. Phys. Chem.* 94 (17), 6820-6825.
- Adav, S.S.; Chen, M.Y.; Lee, D.J.; Ren, N.Q., 2007. Degradation of phenol by aerobic granules and isolated yeast *Candida tropicalis*. *Biotechnol. Bioeng.* 96(5), 844-852.
- Agboola, B.; Ozoemena, K.I.; Nyokong, T., 2005. Hydrogen peroxide oxidation of 2-chlorophenol and 2,4,5-trichlorophenol catalyzed by monomeric and aggregated cobalt tetrasulfophthalocyanine. *J. Mol. Catal. A-Chemical.* 227(1-2), 209-216.
- Aparicio, M.A.; Eiroa, M.; Kennes, C.; Veiga, M.C., 2007. Combined post-ozonation and biological treatment of recalcitrant wastewater from a resin-producing factory. *J Hazard. Mater.* 143(1-2), 285-290.
- Bae, H.S.; Lee J.M.; Lee S.T., 1996. Biodegradation of 4-chlorophenol via a hydroquinone pathway by *Arthrobacter ureafaciens* CPR706. *FEMS Microbiol. Lett.* 145(1), 125-129.
- Bandara, J.; Pulgarin, C.; Peringer, P.; Kiwi, J., 1997. Chemical (photo-activated) coupled biological homogeneous degradation of *p*-nitro-*o*-toluene-sulfonic acid in a flow reactor. *J. Photoch. Photobio. A* 111(1-3), 253-263.
- Belhacova, L.; Krysa, J.; Geryk, J.; Jirkovsky, J., 1999. Inactivation of microorganisms in a flow-through photoreactor with an immobilized TiO₂ layer. *J. Chem. Technol. Biot.* 74(2), 149-154.
- Bergamini, R.B.M.; Azevedo, E.B.; Raddi de Araújo, L.R., 2009. Heterogeneous photocatalytic degradation of reactive dyes in aqueous TiO₂ suspensions: Decolorization kinetics. *Chem. Eng. J.* 149(1-3), 215-220.
- Beydilli, M.I.; Pavlostathis S.G.; Tincher W.C., 2000. Biological decolorization of the azo dye reactive red 2 under various oxidation-reduction conditions. *Water Environ. Res.* 72(6), 698-705.
- Bhatkhande, D.S.; Pangarkar, V.G.; Beenackers, A.A.C.M., 2002. Photocatalytic degradation for environmental applications - a review. *J. Chem. Technol. Biot.* 77(1), 102-116.
- Brunauer, S.; Emmett, P.H.; Teller, E., 1938. Adsorption of gases in multimolecular layers. *J. Am. Chem. Soc.* 60(2), 309-319.

- Cannon, A.S.; Morelli, A.; Pressler, W.; Warner, J.C.; Guarrera, D., 2005. The low temperature processing of titanium dioxide films by the addition of trimesic acid. *J. Sol-Gel Sci. Techn.* 36(2), 157-162.
- Carliell, C.M.; Barclay, S.J.; Naidoo, N.; Buckley, C.A.; Mulholland, D.A.; Senior, E., 1995. Microbial decolourisation of a reactive azo dye under anaerobic conditions. *Water S.A.* 21(1), 61-69.
- Cerniglia, C.E., 1992. Biodegradation of polycyclic aromatic hydrocarbons. *Biodegradation* 3(2-3), 351-368.
- Chatterjee, D.; Patnam, V.R.; Sikdar, A.; Joshi, P.; Misra, R.; Rao, N.N., 2008. Kinetics of the decoloration of reactive dyes over visible light-irradiated TiO₂ semiconductor photocatalyst. *J. Hazard. Mater.* 156(1-3), 435-441.
- Chen, L.C., 2000. Effects of factors and interacted factors on the optimal decolorization process of methyl orange by ozone. *Water Res.* 34(3), 974-982.
- Chen, S.; Sun, D.; Chung, J.S., 2007. Treatment of pesticide wastewater by moving-bed biofilm reactor combined with Fenton-coagulation pretreatment. *J. Hazard. Mater.* 144(1-2), 577-584.
- Cho, I.H.; Zoh, K.D., 2007. Photocatalytic degradation of azo dye (Reactive Red 120) in TiO₂/UV system: Optimization and modeling using a response surface methodology (RSM) based on the central composite design. *Dyes Pigments* 75(3), 533-543.
- Chong, M.N.; Jin, B.; Chow, C.W.; Saint, C., 2010. Recent developments in photocatalytic water treatment technology: a review. *Water Res.* 44(10), 2997-3027.
- Chung, K.T.; Stevens, S.E.J., 1993. Degradation of azo dyes by environmental microorganisms and helminths. *Environ. Toxicol. Chem.* 12(11), 2121-2132.
- Cole, J.R.; Wang, Q.; Cardenas, E.; Fish, J.; Chai, B.; Farris, R.J.; Kulam-Syed-Mohideen, A.S.; McGarrell, D.M.; Marsh, T.; Garrity, G.M.; Tiedje, J.M., 2009. The Ribosomal Database Project: improved alignments and new tools for rRNA analysis. *Nucleic Acids Res.* 37, 141-145.
- Dahlen, E.P.; Rittmann, B.E., 2002a. Two-tank suspended growth process for accelerating the detoxification kinetics of hydrocarbons requiring initial monooxygenation reactions. *Biodegradation.* 13(2), 101-116.
- Dahlen, E.P.; Rittmann, B.E., 2002b. A detailed analysis of the mechanisms controlling the acceleration of 2,4-DCP monooxygenation in the two-tank suspended growth process. *Biodegradation.* 13(2), 117-130.

- Daneshvar, N.; Ayazloo, M.; Khataee, A.R.; Pourhassan, M., 2007. Biological decolorization of dye solution containing Malachite Green by microalgae *Cosmarium* sp.. *Bioresour. Technol.* 98(6), 1176-1182.
- Daneshvar, N. Rabbanib, M.; Modirshahlac, N.; Behnajady, M.A., 2004. Kinetic modeling of photocatalytic degradation of Acid Red 27 in UV/TiO₂ process. *J. Photochem. Photobiol. A: Chem.* 168(1-2), 39-45.
- Daneshvar, N.; Salari, D.; Khataee, A.R., 2003. Photocatalytic degradation of azo dye acid red 14 in water: investigation of the effect of operational parameters. *J. Photochem. Photobiol. A: Chem.* 157(1), 111-116.
- Danion, A.; Bordesb, C.; Disdiera, J.; Gauvritb, J.Y.; Guillardc, C.; Lant érib P.; Jaffrezic-Renaulta, N., 2004. Optimization of a single TiO₂-coated optical fiber reactor using experimental design. *J. Photochem. Photobiol. A: Chem.* 168(3), 161-169.
- Davis, R.J.; Gainer, J.L.; O'Neal, G.; Wu, I.W., 1994. Photocatalytic decolorization of wastewater dyes. *Water Environ.Res.* 66(1), 50-53.
- Faber, M.D., 1979. Microbial degradation of recalcitrant compounds and synthetic aromatic polymers. *Enzyme Microb. Tech.* 1(4), 226-232.
- Fava, F.; Armenante, P.M.; Kafkewitz, D., 1995. Aerobic degradation and dechlorination of 2-chlorophenol, 3-chlorophenol and 4-chlorophenol by a *Pseudomonas pickettii* strain. *Lett. Appl. Microbiol.* 21(5), 307-312.
- Feng, Q.; Zhao, L.; Yan, W.; Lin, J.; Zheng, Z., 2009. Molecularly imprinted solid-phase extraction combined with high performance liquid chromatography for analysis of phenolic compounds from environmental water samples. *J. Hazard. Mater.* 167:282-288.
- Freeman, H.S.; Sokolowska, J., 1999. Developments in dyestuff chemistry. *Rev. Prog. Coloration* 29(1), 8-22.
- Fujishima, A.; Zhang, X.; Tryk, D.A., 2008. TiO₂ photocatalysis and related surface phenomena. *Surf. Sci. Rep.* 63(12), 515-582.
- Genç N., 2004. Photocatalytic oxidation of a reactive azo dye and evaluation of the biodegradability of photocatalytically treated and untreated dye. *Water SA* 30(3), 399-405.
- Grushka, E.; Grinberg, N., 2007. Eds. *Advances in Chromatography, Volume 46*, 1st, ed; CRC Press: Connecticut.

- Haarstrick, A.; Kut, O.M.; Heinzle, E., 1996. TiO₂-assisted degradation of environmentally relevant organic compounds in wastewater using a novel fluidized bed photoreactor. *Enviro. Sci. Technol.* 30(3), 817-824.
- Haas, B.J.; Gevers, D.; Earl, A. M.; Feldgarden, M.; Ward, D. V.; Giannoukos, G.; Ciulla, D.; Tabbaa, D.; Highlander, S.K.; Sodergren, E.; Meth é B.; DeSantis, T.Z.; Human Microbiome Consortium; Petrosino, J.F.; Knight, R.; Birren, B.W., 2011. Chimeric 16S rRNA sequence formation and detection in Sanger and 454-pyrosequenced PCR amplicons. *Genome Res.* 21(3), 494-504.
- H äggblom, M.M., 1992. Microbial Breakdown of Halogenated Aromatic Pesticides and Related-Compounds. *FEMS Microbiol. Rev.* 103(1), 29-71.
- Hofstadler, K.; Rupert, B.; Novalic, S.; Heisler, G., 1994. New reactor design for photocatalytic wastewater treatment with TiO₂ immobilized on fused-silica glass fibers: photomineralization of 4-chlorophenol. *Environ. Sci. Technol.* 28 (4), 670-674.
- Hong, P.K.A.; Zeng, Y., 2002. Degradation of pentachlorophenol by ozonation and biodegradability of intermediates. *Water Res.* 36(17), 4243-4254.
- Horikoshi, S.; Hidaka, H., 2003. Non-degradable triazine substrates of atrazine and cyanuric acid hydrothermally and in supercritical water under the UV-illuminated photocatalytic cooperation. *Chemosphere* 51(2),139-142.
- Huse, S.M.; Huber, J. A.; Morrison, H. G.; Sogin, M. L.; Welch, D. M., 2007. Accuracy and quality of massively parallel DNA pyrosequencing. *Genome Biol.* 8(7), R143.
- Itoh, K.; Tashiro, Y.; Uobe, K.; Kamagata, Y.; Suyama, K.; Yamamoto, H., 2004. Root Nodule *Bradyrhizobium* spp. Harbor *tfdAa* and *cadA*, Homologous with Genes Encoding 2,4-Dichlorophenoxyacetic Acid-Degrading Proteins. *Appl. Environ. Microbiol.* 70(4), 2110-2118.
- Jadhav, J.P.; Parshetti, G.K.; Kalme, S.D.; Govindwar, S.P., 2007. Decolourization of azo dye methyl MTCC red by *Saccharomyces cerevisiae* MTCC-463. *Chemosphere* 68(2), 394-401.
- Jiang, X.; Liu, H.; Xu, Y.; Wang, S.; Leak, D.; Zhou, N., 2009. Genetic and biochemical analyses of chlorobenzene degradation gene clusters in *Pandora* sp. strain MCB032. *Arch. Microbiol.* 191(6), 485-492.
- Kritikos, D.E.; Xekoukoulotakis, N.P.; Psillakis, E.; Mantzavinos, D., 2007. Photocatalytic degradation of reactive black 5 in aqueous solutions: Effect of operating conditions and coupling with ultrasound irradiation. *Water Res.* 41(10), 2236-2246.

- Lee, C.; Yoon, J., 2004. Application of photoactivated periodate to the decolorization of reactive dye: reaction parameters and mechanism. *J. Photochem. Photobiol. A: Chem.* 165(1-3), 35-41.
- Lee, H.S.; Parameswarana, P.; Marcus, A.K.; Torres, C.I.; Rittmann, B.E., 2008. Evaluation of energy-conversion efficiencies in microbial fuel cells (MFCs) utilizing fermentable and non-fermentable substrates. *Water Res.* 42(6-7), 1501-1510.
- Li, X.; Cabbage, J.W.; Tetzlaff, T.A.; Jenks, W.S., 1999. Photocatalytic degradation of 4-chlorophenol. 1. The hydroquinone pathway. *J. Org. Chem.* 64 (23), 8509-8524.
- Mao, Y.; Zhang, X.; Yan, X.; Liu, B.; Zhao, L., 2008. Development of group-specific PCR-DGGE fingerprinting for monitoring structural changes of *Thauera* spp. in an industrial wastewater treatment plant responding to operational perturbations. *J. Microbiol. Methods* 75(2), 231-236.
- Marco, A.; Esplugas, S.; Saum, G., 1997. How and why to combine chemical and biological processes for wastewater treatment. *Water Sci. Technol.* 35(4), 321-327.
- Marsolek, M.D.; Kirisits, M.J.; Rittmann, B.E., 2007. Biodegradation of 2,4,5-trichlorophenol by aerobic microbial communities: biorecalcitrance, inhibition, and adaptation. *Biodegradation* 18(3), 351-358.
- Marsolek, M.D.; Torres C.I.; Hausner M.; Rittmann B.E., 2008. Intimate coupling of photocatalysis and biodegradation in a photocatalytic circulating-bed biofilm reactor. *Biotechnol. Bioeng.* 101(1), 83-92.
- Miller, R.M.; Singer, G. M.; Rosen J. D.; Bartha, R., 1988. Sequential degradation of chlorophenols by photolytic and microbial treatment. *Environ. Sci. Technol.* 22(10), 1215-1219.
- Mohan, D.; Singh, K.P.; Singh, G.; Kumar, K., 2002. Removal of dyes from wastewater using fly ash, a low-cost adsorbent. *Ind. Eng. Chem. Res.* 41(15), 3688-3695.
- Morgan-Sagastume, F.; Nielsen, J.L.; Nielsen, P.H., 2008. Substrate-dependent denitrification of abundant probe-defined denitrifying bacteria in activated sludge. *FEMS Microbiol. Ecol.* 66(2), 447-461.
- Mutambanengwe, C.C.; Togo, C.A.; Whiteley, C.G., 2007. Decolorization and degradation of textile dyes with biosulfidogenic hydrogenases. *Biotechnol. Prog.* 23(5), 1095-1100.

- Nigam, P.; Armour, G.; Banat, I.M.; Singh, D.; Marchant, R., 2000. Physical removal of textile dyes from effluents and solid-state fermentation of dye-adsorbed agricultural residues. *Bioresour. Technol.* 72(3), 219-226.
- Nishio, J.; Tokumura, M.; Znad, H. T.; Kawase, Y., 2006. Photocatalytic decolorization of azo-dye with zinc oxide powder in an external UV light irradiation slurry photoreactor. *J Hazard. Mater.* 138(1).106-115.
- Nitschke, L.; Schüssler, W., 1998. Surface water pollution by herbicides from effluents of waste water treatment plants. *Chemosphere* 36(1), 35-41.
- Özen, A.S.; Aviyente V., 2003. Modeling the Oxidative Degradation of Azo Dyes: A Density Functional Theory Study. *J. Phys. Chem. A* 107(24), 4898-4907.
- Pruesse, E.; Quast, C.; Knittel, K.; Fuchs, B.M.; Ludwig W.; Peplies, J.; Glöckner, F.O., 2007. SILVA: a comprehensive online resource for quality checked and aligned ribosomal RNA sequence data compatible with ARB. *Nucleic Acids Res.* 35(21), 7188-7196.
- Renfrew, A., 1999. Reactive Dyes for Textile Fibres. *The Society of Dyers and Colourists*: Bradford, UK.
- Ribeiro, M.H.L.; Lourenço, P.A.S.; Monteiro, J.P.; Ferreira-Dias, S., 2001. Kinetics of selective adsorption of impurities from a crude vegetable oil in hexane to activated earths and carbons. *Eur. Food Res. Technol.* 213(2), 132-138.
- Roberts, G.W.; Satterfield, C.N., 1965. Effectiveness Factor for Porous Catalysts: Langmuir-Hinshelwood Kinetic Expressions. *Ind. Eng. Chem. Fundamen.* 4 (3), 288-293.
- Rodgers, J.D.; Bunce, N.J., 2001. Treatment methods for the remediation of nitroaromatic explosives. *Water Res.* 35(9), 2101-2111.
- Rodriguez, S.M.; Galvez, J.B.; Rubio, M.I.; Ibanez, P.F.; Gernjak, W.; Alberola, I.O., 2005. Treatment of chlorinated solvents by TiO₂ photocatalysis and photo-Fenton: Influence of operating conditions in a solar pilot plant. *Chemosphere* 58(4), 391-398.
- Sambrook, J.; Russell, D., 2001. *Molecular cloning: a laboratory manual*, 3rd ed.; Cold Spring Harbor Laboratory Press: New York.
- Sandrint, T.R.; Maier, R.M., 2002. Effect of pH on cadmium toxicity, speciation, and accumulation during naphthalene biodegradation. *Environ. Toxicol. Chem.* 21(10), 2075-2079.

- Schloss, P.D.; Westcott, S.L.; Ryabin, T.; Hall, J.R.; Hartmann, M.; Hollister, E.B.; Lesniewski, R.A.; Oakley, B.B.; Parks, D.H.; Robinson, C.J.; Sahl, J.W.; Stres, B.; Thallinger, G.G.; Van Horn, D.J.; Weber, C.F., 2009. Introducing mothur: Open-source, platform-independent, community-supported software for describing and comparing microbial communities. *Appl. Environ. Microb.* 75(23), 7537-7541.
- Schwien, U.; Schmidt, E.; Knackmuss, H.J.; Reineke, W., 1988. Degradation of chlorosubstituted aromatic compounds by *Pseudomonas* sp. strain B13: fate of 3,5-dichlorocatechol. *Arch. Microbiol.* 150(1), 78-84.
- Scott, J.P.; Ollis, D.F., 1995. Integration of chemical and biological oxidation processes for water treatment: Review and recommendations. *Environ. Prog.* 14(2), 88-103.
- Scott, J.P.; Ollis, D.F., 1996. Engineering models of combined chemical and biological processes. *J. Environ. Eng.* 122(12), 1110-1114.
- Sirtori, C.; Zapata, A.; Oller, I.; Gernjak, W.; Agüera, A.; Malato, S., 2009. Decontamination industrial pharmaceutical wastewater by combining solar photo-Fenton and biological treatment. *Water Res.* 43(3), 661-668.
- Skurlatov, Y.I.; Ernestova, L.S.; Vichutinskaya, E.V.; Samsonov, D.P.; Semenova, I.V.; Rod'ko, I.Y.; Shvidky, V.O.; Pervunina, R.I.; Kemp, T.J., 1997. Photochemical transformation of polychlorinated phenols. *J. Photoch. Photobio. A* 107(1-3), 207-213.
- Sponza, D.T.; Işık, M., 2002. Decolorization and azo dye degradation by anaerobic/aerobic sequential process. *Enzyme Microb. Technol.* 31(1-2), 102-110.
- Staples, C.A.; Dorn, P.B.; Klecka, G.M.; O'Block, S.T.; Harris, L.R., 1998. A review of the environmental fate, effects, and exposures of bisphenol A. *Chemosphere* 36(10), 2149-2173.
- Steady, C.V., 1982. Halogenated heterocycles in reactive dyes. *Dyes Pigments* 3(2-3), 161-171.
- Steinle, P.; Stucki, G.; Stettler, R.; Hanselmann, K.W., 1998. Aerobic mineralization of 2,6-dichlorophenol by *Ralstonia* sp. strain RK1. *Appl. Environ. Microb.* 64(7), 2566-2571.
- Taylor, J.A., 2000. Recent Developments in Reactive Dyes. *Rev. Prog. Coloration* 30(1), 93-107.

- U.S. Environmental Protection Agency, 1994. Health Effects Notebook, for Hazardous Air Pollutants, 2,4,5-Trichlorophenol. Washington, D.C.: Office of Air Quality Planning and Standards,
- Valderrama, L.T.; Del Campo, C.M.; Rodriguez, C.M.; de-Bashan, L.E.; Bashan, Y., 2002. Treatment of recalcitrant wastewater from ethanol and citric acid production using the microalga *Chlorella vulgaris* and the macrophyte *Lemna minuscula*. *Water Res.* 36(17), 4185-4192.
- Wang, H.; Zheng, X. W.; Su, J.Q.; Tian, Y.; Xiong, X.J.; Zheng, T.L., 2009. Biological decolorization of the reactive dyes Reactive Black 5 by a novel isolated bacterial strain *Enterobacter* sp EC3. *J. Hazard. Mater.* 171(1-3), 654-659.
- Weber, E.J.; Stickney, V.C., 1993. Hydrolysis kinetics of Reactive Blue 19-Vinyl Sulfone. *Water Res.* 27(1), 63-67.
- Wolcott, R.D.; Gontcharova, V.; Sun, Y.; Dowd, S.E., 2009. Evaluation of the bacterial diversity among and within individual venous leg ulcers using bacterial tag-encoded FLX and titanium amplicon pyrosequencing and metagenomic approaches. *BMC Microbiol.* 9, 226; DOI 10.1186/1471-2180-9-226.
- Won, S.W.; Han, M.H.; Yun, Y.S., 2008. Different binding mechanisms in biosorption of reactive dyes according to their reactivity. *Water Res.* 42(19), 4847-4855.
- Zhang, B.; Ji, M.; Qiu, Z.; Liu, H.; Wang, J.; Li, J., 2011. Microbial population dynamics during sludge granulation in an anaerobic-aerobic biological phosphorus removal system. *Bioresource Technol.* 102(3), 2474-2480.

